Calhoun: The NPS Institutional Archive

DSpace Repository

Theses and Dissertations | 1. Thesis and Dissertation Collection, all items

1992-06

A theory for whistler wave amplification and wave particle interactions in the magnetosphere

Gately, Bernard M.

Monterey, California. Naval Postgraduate School

https://hdl.handle.net/10945/38526

This publication is a work of the U.S. Government as defined in Title 17, United States Code, Section 101. Copyright protection is not available for this work in the United States.

Downloaded from NPS Archive: Calhoun

http://www.nps.edu/library

Calhoun is the Naval Postgraduate School's public access digital repository for research materials and institutional publications created by the NPS community. Calhoun is named for Professor of Mathematics Guy K. Calhoun, NPS's first appointed -- and published -- scholarly author.

Dudley Knox Library / Naval Postgraduate School
411 Dyer Road / 1 University Circle
Monterey, California USA 93943

AD-A257 782

(2)

NAVAL POSTGRADUATE SCHOOL
Monterey, California

DTIC
ELECTE
DEC 8 1992
S C D

THESIS

A THEORY FOR WHISTLER WAVE AMPLIFICATION
AND WAVE PARTICLE INTERACTIONS
IN THE MAGNETOSPHERE

by

Bernard M. Gately Jr.

June 1992

Thesis Advisor: W. B. Colson

approved for public release; distribution is unlimited.

92-31056

REPORT DOCUMENTATION PAGE

Form Approved
OMB No. 0704-0188

1a REPORT SECURITY CLASSIFICATION: UNCLASSIFIED	1b RESTRICTIVE MARKINGS
2a SECURITY CLASSIFICATION AUTHORITY: Multiple Sources	3 DISTRIBUTION / AVAILABILITY OF REPORT: Approved for public release; distribution is unlimited
2b DECLASSIFICATION / DOWNGRADING SCHEDULE: (OADR)	
4 PERFORMING ORGANIZATION REPORT NUMBER(S)	5 MONITORING ORGANIZATION REPORT NUMBER(S)
6a NAME OF PERFORMING ORGANIZATION: Naval Postgraduate School; 6b OFFICE SYMBOL (If applicable): 33	7a NAME OF MONITORING ORGANIZATION: Naval Postgraduate School
6c ADDRESS (City, State, and ZIP Code): Monterey, CA 93940-5000	7b ADDRESS (City, State, and ZIP Code): Monterey, CA 93940-5000
8a NAME OF FUNDING / SPONSORING ORGANIZATION; 8b OFFICE SYMBOL (If applicable)	9 PROCUREMENT INSTRUMENT IDENTIFICATION NUMBER
8c ADDRESS (City, State, and ZIP Code)	10 SOURCE OF FUNDING NUMBERS: PROGRAM ELEMENT NO; PROJECT NO; TASK NO; WORK UNIT ACCESSION NO

11 TITLE (Include Security Classification): A THEORY FOR WHISTLER WAVE AMPLIFICATION AND WAVE PARTICLE INTERACTIONS IN THE MAGNETOSPHERE

12 PERSONAL AUTHOR(S): Gately, Bernard M., Jr.

13a TYPE OF REPORT	13b TIME COVERED	14 DATE OF REPORT (Year, Month, Day)	15 PAGE COUNT
Master's thesis	FROM _____ TO _____	June 1992	70

16 SUPPLEMENTARY NOTATION: The views expressed in this thesis are those of the author and do not reflect the official policy or the position of the Department of Defense or the U. S. Government

17 COSATI CODES			18 SUBJECT TERMS (Continue on reverse if necessary and identify by block number)
FIELD	GROUP	SUB-GROUP	WHISTLERS, WHISTLER WAVES, WAVE PARTICLE INTERACTIONS

19 ABSTRACT (Continue on reverse if necessary and identify by block number)

Whistler waves are a type of very low frequency (VLF) radiation which propagate through the earth's magnetosphere. This phenomenon can occur as a result of a lightning discharge and can be produced using ground-based VLF transmitters. It is theorized that these signals travel through ducts centered on geomagnetic field lines. While passing through these ducts the waves are amplified through resonant interaction with electrons in the radiation belts which are following helical paths around magnetic field lines. A description of whistlers and the related topic of VLF emissions is presented in Chapter II, along with a description of how these effects change the properties of the ionosphere.

20 DISTRIBUTION / AVAILABILITY OF ABSTRACT: ☒ UNCLASSIFIED/UNLIMITED ☐ SAME AS RPT ☐ DTIC USERS	21 ABSTRACT SECURITY CLASSIFICATION: Unclassified
22a NAME OF RESPONSIBLE INDIVIDUAL: W. B. Colson	22b TELEPHONE (Include Area Code): (408) 646-2765; 22c OFFICE SYMBOL: 61

19.

Starting with the Lorentz force equation, the equations of motion for electrons in the magnetosphere are developed in Chapter III. These equations are numerically integrated along with a wave equation developed in Chapter IV. The results of the simulation are presented in Chapter V for the idealized case of a monoenergetic beam of electrons. High and low gains in the wave amplitude are observed for both strong and weak initial VLF fields. The simulation is also run using distributions to represent the initial energies of the electrons in the radiation belts. Chapter VI presents some possible ways to make the simulation more realistic along with a summary of the similarities between the theory presented and Free Electron Laser theory.

Approved for public release; distribution is unlimited.

A THEORY FOR WHISTLER WAVE AMPLIFICATION AND WAVE PARTICLE INTERACTIONS IN THE MAGNETOSPHERE

by

B. M. Gately Jr.

Lieutenant, United States Navy

B. S., United States Naval Academy, 1986

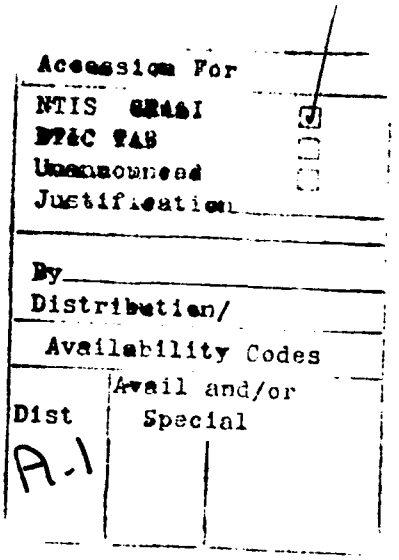

Submitted in partial fulfillment of the

requirements for the degree of

MASTER OF SCIENCE IN PHYSICS

from the

NAVAL POSTGRADUATE SCHOOL

June 1992

Author: [redacted]

Bernard M. Gately Jr.

Approved by: [redacted]

William B. Colson, Thesis Advisor

[redacted]

Suntharalingam Gnanalingam, Second Reader

[redacted]

Karlheinz E. Woehler, Chairman,

Department of Physics

ABSTRACT

Whistler waves are a type of very low frequency (VLF) radiation which propagate through the earth's magnetosphere. This phenomenon can occur as a result of a lightning discharge and can be produced using ground-based VLF transmitters. It is theorized that these signals travel through ducts centered no geomagnetic field lines. While passing through these ducts the waves are amplified through resonant interaction with electrons in the radiation belts which are following helical paths around magnetic field lines. A description of whistlers and the related topic of VLF emissions is presented in Chapter II, along with a description of how these effects change the properties of the ionosphere.

Starting with the Lorentz force equation, the equations of motion for electrons in the magnetosphere are developed in Chapter III. These equations are numerically integrated along with a wave equation developed in Chapter IV. The results of the simulation are presented in Chapter V for the idealized case of a monoenergetic beam of electrons. High and low gains in the wave amplitude are observed for both strong and weak initial VLF fields. The simulation is also run using distributions to represent the initial energies of the electrons in the radiation belts. Chapter VI presents some possible ways to make the simulation more realistic along with a summary of the similarities between the theory presented and Free Electron Laser theory.

Table of Contents

I. INTRODUCTION 1

II. VLF RADIATION IN THE MAGNETOSPHERE 3

A. WHISTLERS 3

B. VLF EMISSIONS 9

C. EFFECTS OF VLF EMISSIONS 13

III. THE ENVIRONMENT AND EQUATIONS OF MOTION 16

A. THE MAGNETOSPHERE 16

B. THE MAGNETIC FIELD 18

C. ELECTRON MOTION IN THE MAGNETOSPHERE 20

D. ELECTRON EQUATIONS OF MOTION IN A MAGNETIC FIELD 24

IV. WAVE PARTICLE INTERACTION THEORY 27

A. THE BACKGROUND PLASMA 27

B. THE WAVE EQUATION 30

C. DEVELOPMENT OF ELECTRON EQUATIONS OF MOTION 33

V. SIMULATION AND DISCUSSION 37

A. EXPLAINATION OF NUMERICAL INTEGRATION METHODS 37

B. INITIAL CONDITIONS 38

C. INTERACTION FOR MONO-ENERGETIC BEAM 39

D. SIMULATION USING DISTRIBUTIONS 48

VI. SUGGESTIONS FOR FUTURE WORK 52

A. IMPROVEMENTS TO THE SIMULATION 52

B. COMPARISON TO FREE ELECTRON LASERS 54

VII. CONCLUSIONS 56

LIST OF REFERENCES 58

INITIAL DISTRIBUTION LIST 61

ACKNOWLEDGEMENT

The author gratefully acknowledges the assistance, guidance and friendship provided by Dr. W. B. Colson. He would also like to thank Mr. J. Blau, LT D. Caudle USN and CAPT K. Strugess USA for all the help they provided during the preparation of this thesis. The author wishes to express his gratitude for the loving support and patience of his family; Marie, Colleen and my wife and best friend, Karen.

I. INTRODUCTION

The study of "whistlers" dates back to the earliest days of radio communications. The first reported survey of these distinct musical type signals came about as a result of German attempts to listen in on Allied telephone conversations during World War I [1]. From these beginnings, has developed a theory of how whistlers are produced and how the waves propagate between magnetic conjugant points in the Northern and Southern hemisphere. This information is reviewed in Chapter II of this thesis. The study of the related phenomenon of VLF emissions dates back to the early 1950's and a review of this theory is also presented in Chapter II. The chapter concludes with a look at how these signals can limit the range of VLF communication systems and degrade the accurracy of the navigation systems used by the U. S. Navy

In Chapter III a description of the magnetosphere is provided. Most of the early information on this region of space comes from the study of whistler spectrograms. Chapter III concludes with a discussion about the electrons in the magnetosphere along with the equations of motion used to describe how the electrons move in the geomagnetic field.

A theory proposed to explain the amplification of VLF signals in the magnetosphere is that of wave-particle interactions between incoming VLF waves and a stream of counter-propagating electrons. This resonant interaction is thought to occur in a region of space within a few degrees above and below the geomagnetic equator, and at geocentric distances of three to six earth radii. The rest of the thesis explores this nonlinear interaction through the use of computer simulations. In Chapter IV, background plasma in the interaction

region is described which leads to a wave equation used to follow the development of the amplitude and phase of the wave as it passes through the interaction region. The motion of the resonant electrons in the presence of the wave is described using a set of first order differential equations which are developed from the Lorentz force equation.

The computer simulation numerically integrates the electron equations of motion and the wave equation given a set of initial conditions. In Chapter V, the results of this simulation are presented for a variety of initial conditions. The first set of simulations explore what happens for the case of a monoenergetic beam of electrons. Conditions needed to produce high and low gain in the wave are explored as well as strong and weak fields. The second set of runs uses initial conditions which approximate those found in the ionospheric interaction region. The initial phase velocities and transverse velocities for the resonant electrons are determined using distribution functions.

In Chapter VI, suggestions for future work to improve the simulation is discussed. It turns out that the theory presented in this thesis regarding wave-particle intercations has many similarities to the theory used to describe the Free Electron Laser. These similarities are discussed at the end of Chapter VI.

II. VLF RADIATION IN THE MAGNETOSPHERE

A. WHISTLERS

"Whistler waves" are one type of very low frequency (VLF) electromagnetic radiation which propagate through the earth's magnetosphere and are detected at magnetically conjugate points on the earth's surface. The name "whistler" provides the best description of what these emissions sound like; a high pitched tone (in the kilohertz range) which sweeps down in frequency over the period of about one second. Whistlers can be heard by the human ear using very simple equipment. As a result, reports of their occurrence date back to the earliest radio experiments. Two metal probes placed in the ground 50 feet apart and connected to a high gain amplifier makes an excellent whistler receiver. They can also be heard over telephones connected to long telephone lines. The rate of whistler activity varies with the time of day, magnetic activity and location on the earth. They are more common at night and frequently occur in conjunction with lightning storms. Mid-latitude regions report the highest rate of whistler activity, while lower rates are found in the higher latitudes. Whistlers have not been observed at the equator or at the poles. The latitudes where the highest rates are reported seem to move toward the equator during periods of increased magnetic activity.[1]

The close association between lightning discharges and the detection of whistlers has lead to the following explanation for the occurrence of these waves. A lightning discharge releases radio waves with a wide-band of frequencies. Some of these waves reflect off the ionosphere, at altitudes

between 90 and 200 kilometers (km) and can travel over the horizon to ranges of thousands of kilometers. It is postulated that some of the radiation from the lightning penetrates the ionosphere and enters ducts which are centered on geomagnetic field lines. The waves follow these field-aligned ducts from one hemisphere to the magnetic conjugate point in the other hemisphere. The waves pass through the ionosphere and are detected as whistlers. The distinctive falling pitch indicates that the path taken by the whistlers is highly dispersive. Higher frequency components of the wave travel faster through the ducts than those with a lower frequency, arriving at the receiver first. A portion of the wave can also reflect off the top of the ionosphere, returning to the originating hemisphere along the same duct. This "two-hop" whistler is then detected at a ground receiver. This reflection between magnetic conjugate points can occur many times and produce a number of echos.[2] In addition to lightning, VLF radiation from a nuclear explosion and man-made Morse code dashes from VLF transmitters can all travel in this same whistler mode [1].

The ducts which whistlers travel through are believed to work on the same principles as a fiber optic cable. There is a region around the magnetic field line of increased electron density. This results in a higher index of refraction and the electromagnetic waves tend to stay within this region due to total internal reflection, as long as the angle of incidence between the wave and the wall of the duct is small. Extensive study of whistler data have shown that the time between successive whistler echos at one receiver is always an integral number of seconds. In addition, the dispersion properties of two whistlers do not change over the course of many minutes indicating that the whistlers travel the same path. These results reinforce the theory that the waves follow ducts which are aligned with magnetic field lines.[3]

A convenient way to display whistlers is with a frequency verses time spectrogram shown in Figure 2-1. The small arrow indicates reception of the impulse which causes the whistler, possibly a stroke of lightning in the case of naturally occurring whistlers. The dark, curved trace indicates reception of the

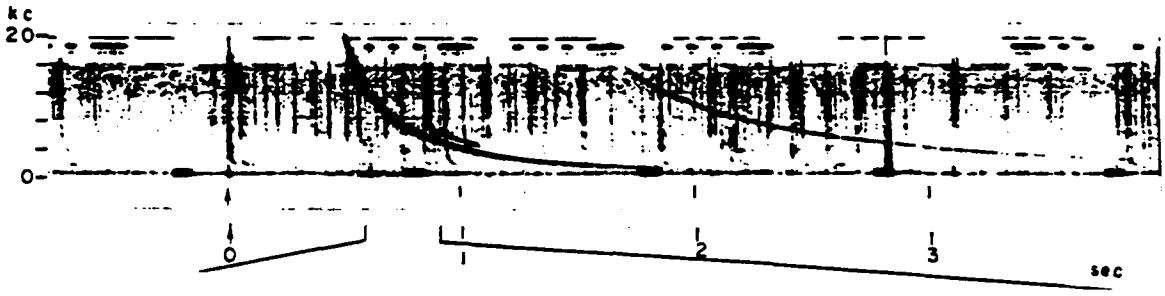

Figure 2-1: Whistler spectrogram on a frequency versus time scale [1].

whistler signal. The darker the line the higher the intensity received. The time delay between the impulse and reception of the whistler is proportional to the length of the whistler's path of propagation. In this case the first trace is a one-hop whistler. It has made one pass through the duct. The smooth decrease in frequency is clearly evident. Also shown in Figure 2-1 is an echo or "three-hop" whistler which has made three trips through the same field aligned duct before passing through the ionosphere and being picked up by the receiver. The rate of frequency decrease in this and succeeding whistler echos is not as great as in the initial whistler trace. Each successive echo makes one more pass through the dispersive medium in the duct then the previous echo, stretching out the spectrogram for each successive echo.[1]

The initiating lightning impulse does not sweep in frequency because it travels by a direct path in the earth ionosphere waveguide to the receiver. Very little dispertion takes place below the ionosphere and the travel time for the impulse is a fraction of a second resulting in a spike made up of many frequencies and very short in duration.[1]

Figure 2-2 shows a group of whistlers packed very close together. These are an examples of "multipath whistlers". Some of the energy coming from a particular lightning stroke can enter adjacent ducts, each with a slightly different path length. As a result the waves have different travel times and when received appear to overlap as shown in Figure 2-2.[4]

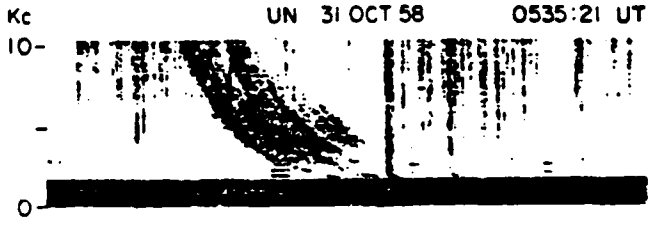

Figure 2-2: Example of multipath whistlers [1].

$$t(\omega) = \int \frac{ds}{v_g} \qquad 2\text{-}1$$

where v_g is the whistler group velocity and ds is an increment of path length. This travel time is a function of frequency (ω) because plasma in the duct provides a dispersive medium. Assuming that the group velocity is constant over the total path, it can be taken out of the integral and written as

$$v_g = \frac{c}{n_g} \qquad 2\text{-}2$$

where c is the speed of light in a vacuum and n_g is the group index of refraction which is defined as $n_g = n + \omega\, dn/d\omega$. The index of refraction, n, is also a function of frequency and is known to have the form [3]

$$n \approx \frac{\omega_c}{\sqrt{\omega(\Omega-\omega)}}, \qquad 2\text{-}3$$

where the plasma frequency, ω_c, and the electron cyclotron frequency, Ω, are defined as

$$\omega_c = \left[\frac{4\pi e^2 \rho}{m}\right]^{\frac{1}{2}} \quad \text{and} \quad \Omega = \frac{eB}{mc}\ , \qquad 2\text{-}4$$

where e is the electron charge magnitude, B is the magnitude of the magnetic field, m is the electron mass and ρ is the electron density. The approximation stated in equation 2-3 is accurate for the case where $\omega_c >> \omega$ and $\omega_c >> \Omega$. This situation exists for the region where whistlers propagate. Assuming that the waves follow a particular geomagnetic line of force and that the earth's magnetic field is a dipole, the path length can be determined [1]. The resulting equation for travel time is

$$t(\omega) = \frac{l}{2c}\frac{\omega_c \Omega}{\omega^{1/2}}(\Omega-\omega)^{-3/2}\ . \qquad 2\text{-}5$$

where l is the total path length.[5]

Figure 2-3 is a plot of $t(\omega)$. In this graph, frequency is normalized to the electron cyclotron frequency and time is given in seconds. Also indicated is the frequency of minimum time delay, know as the "nose frequency" ω_n. It can be shown using the equation for $t(\omega)$ that a relationship exists between ω_n and Ω:

$$\omega_n = 0.25\Omega \quad . \qquad 2\text{-}6$$

Substituting this value back into the equation for $t(\omega)$ results in an expression for the nose time delay t_n:

$$t_n = \frac{8\sqrt{3}\ l\ \omega_c}{3\ c\ \Omega} \quad . \qquad 2\text{-}7$$

This derivation results in a way to find Ω using the value for ω_n which is read from the nose whistler spectrogram. Then for a given path length l, the plasma frequency ω_c can be determined using equation 2-7. This analysis assumes the plasma in the magnetosphere is uniformly distributed.[5]

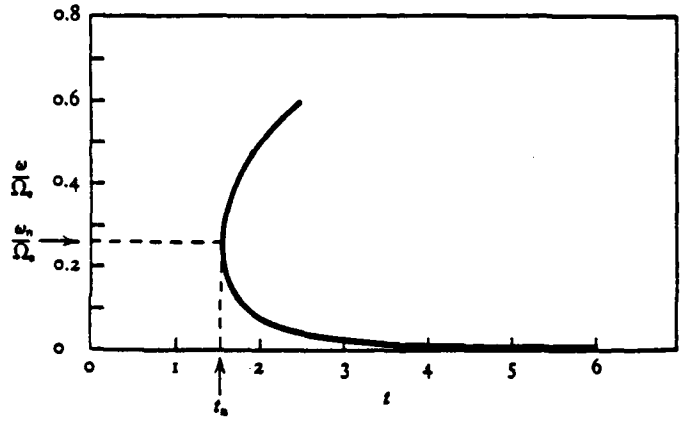

Figure 2-3: Plot of $t(\omega)$ [5].

The real magnetosphere does not completely comply with the assumptions made in the preceding analysis. Extensive study of nose whistlers, such as pictured in Figure 2-4, has lead to an accurate relationship between ω_n and Ω:

$$\omega_n = 0.40\Omega \ . \qquad 2\text{-}8$$

Nose whistler analysis has lead to the discovery of a reduction in electron concentration at an altitude of four earth radii above the geomagnetic equator. This region is know as the plasmapause, and its position as a function of geomagnetic activity can be tracked using nose whistlers [6].

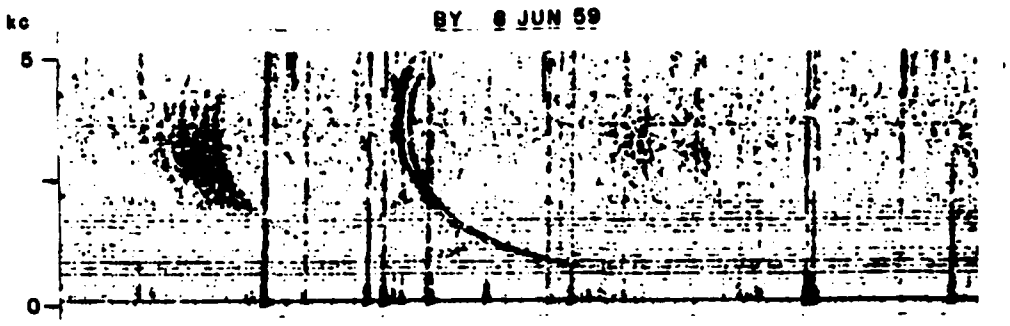

Figure 2-4: Nose whistler spectrogram [1].

B. VLF EMISSIONS

A second type of wave that propagates through the magnetosphere is known as a VLF emission. These waves fall into two major categories, "hiss" shown in Figure 2-5 and discrete emissions also shown in Figure 2-5 and which go by the names "risers", "fallers" and "hooks" [1]. Hiss is broad band low frequency radiation which has a definite cut-off frequency. The various types of discrete emissions are narrow band and can sweep through a range of frequencies over the period of a second. The same equipment is used in the study of VLF emissions as is used to detect whistlers. VLF emissions can

occur in conjunction with strong whistlers. A whistler can trigger a discrete emission such as in Figure 2-6, where the emission begins at the low frequency tail of the whistler. These types of whistler triggered emissions are more frequent during periods of high magnetic activity and are limited to the higher latitudes. In the polar regions, VLF emissions can significantly degrade the performance of communications systems. They exhibit the same level of intensity as whistlers and are also more common in middle to higher latitudes. There is a close relationship in form and time between emissions detected at magnetic conjugate points on the earth's surface. This observation has led to the theory that the waves travel through the magnetosphere in the same manner described for whistlers. This is known as the whistler-mode of propagation. There is also strong association between auroral activity and an increase in VLF emission rates.[1]

The sources of VLF emissions are not completely understood. They probably originate in the magnetosphere and are the result of the interaction between waves propagating in the whistler-mode and high energy electrons (keV) located in the radiation belts which spiral around geomagnetic field lines. In addition to whistler triggered emissions it has been found that ground based VLF transmitters can produce triggered emissions as shown in Figure 2-7. Extensive research using these man-made triggered emissions has led to the following list of characteristics:

1. A minimum pulse length is needed to produce a triggered emission. Only Morse code dashes of length 100-150 ms result in an emission, Morse code dots of length 50ms do not trigger an emission.

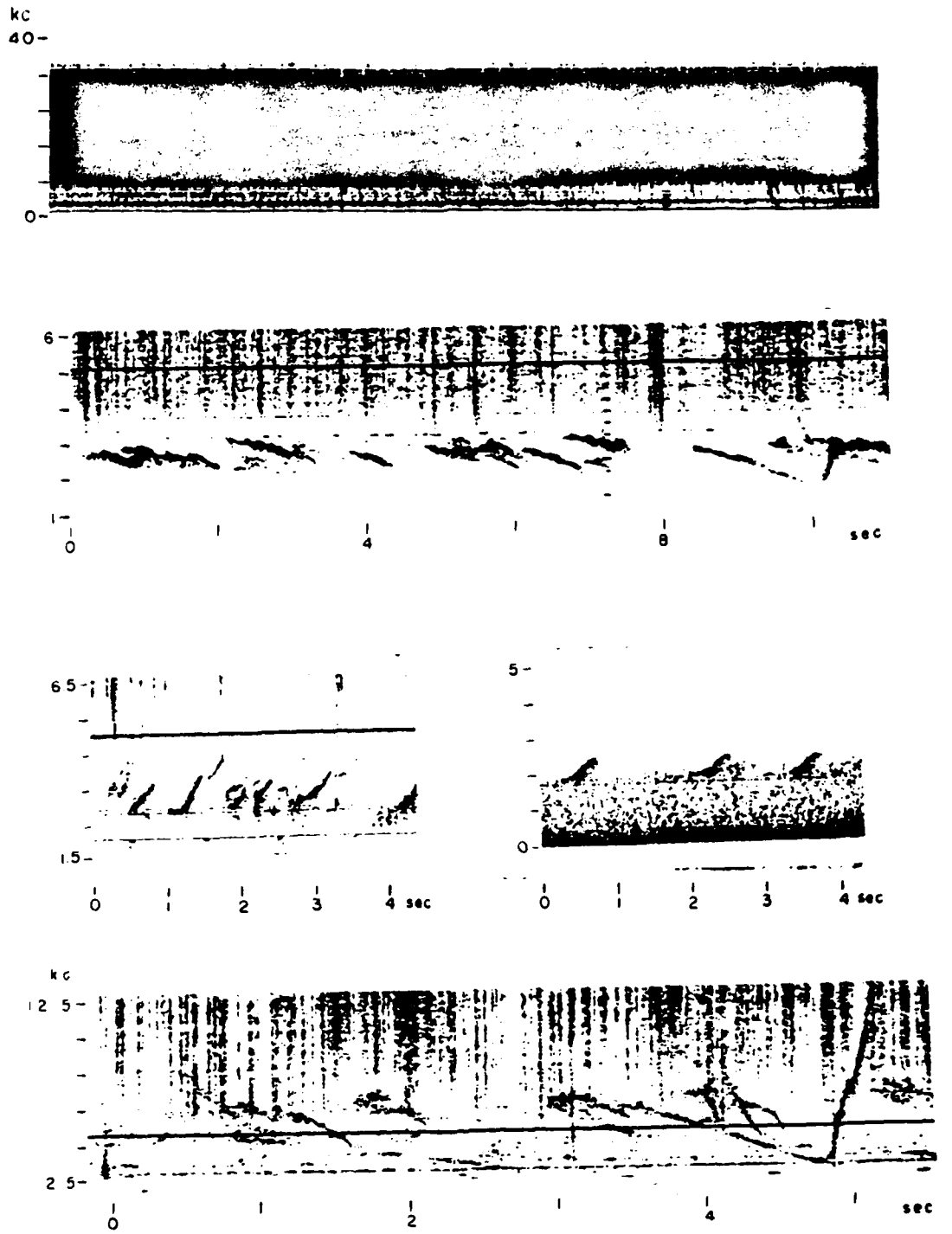

Figure 2-5: Examples of VLF emissions (from top); "hiss", "fallers", "risers" and "hooks" [1].

2. The original VLF signal shows growth in intensity on the order of 25-30 dB prior to the triggered emission. The triggered emission starts once the initiating signal stops. Observations of triggered emissions caused by whistlers shows that the triggered signal begins toward the end of the whistler pulse in the range where the rate of frequency decrease is a minimum.

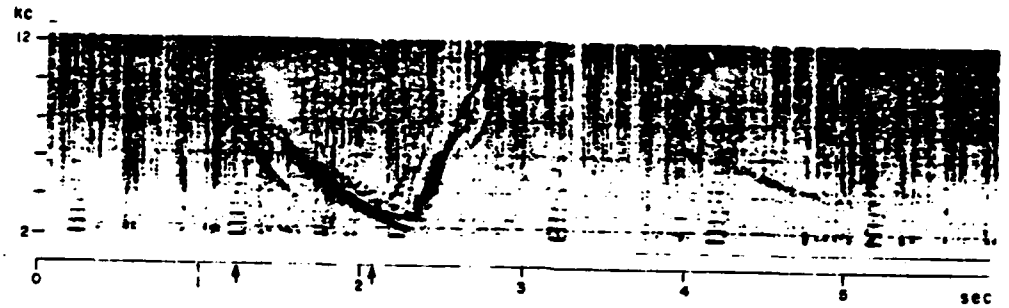

Figure 2-6: Example of a whistler triggered VLF emission in this case a hook [1].

3. The triggered signal begins at (or within 200HZ of) the frequency of the initiating pulse and sweeps up or down in frequency in a fraction of a second. The longer the initial pulse the more likely that a riser will result. The emission in extremely narrow band (≈100Hz) and the sweeping frequency change can be as much as 50%. The triggered signal also tends to end abruptly.

4. There are occasions when triggered emissions do not occur when a Morse code dash is transmitted. The reason for this is not known but the gain and frequency variation described above, when a triggered emission does occur, "are relatively insensitive" to the level of geomagnetic activity.[7]

D. EFFECTS OF VLF EMISSIONS

The interaction which causes VLF emissions is also considered to be the mechanism that causes high energy electrons to precipitate out of the earth's radiation belts. The electron spiral motion around the magnetic field lines couples with VLF waves and amplifies them. This process reduces the energy

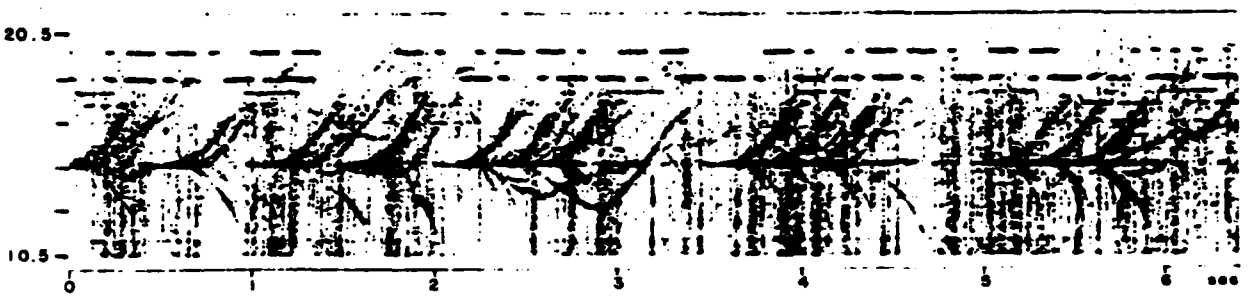

Figure 2-7: A constant 14.7kHz signal and the resulting triggered emissions. In this case risers, fallers and hooks are generated [1].

of the electrons and causes them to enter the ionosphere. These high energy electrons can increase the plasma frequency in the low levels of the ionosphere directly through ionization or indirectly through the production of bremmstrahlung x-rays or ultraviolet emissions. The result of this is the formation of a "pimple" protruding down from the bottom boundary of the ionosphere as illustrated in Figure 2-8 [9]. VLF waves passing through the earth-ionosphere wave guide can scatter off this region, adding constructively and destructively to the unscattered wave and resulting in changes to the amplitude and phase of the original signal. This phenomenon, known as a "Trimpi event" [10] is well documented and can be initiated by naturally occurring whistlers which then trigger VLF emissions and by ground-based VLF transmitters.

The VLF communication systems and radio navigation systems used by the U. S. Navy are susceptible to changes in the ionosphere produced by the Trimpi effect. One such system is the Omega radio navigation system in which a user determines his distance from a particular transmitter by comparing the phase difference between two signals of the same frequency sent out from two different locations. There are eight Omega stations throughout the world each

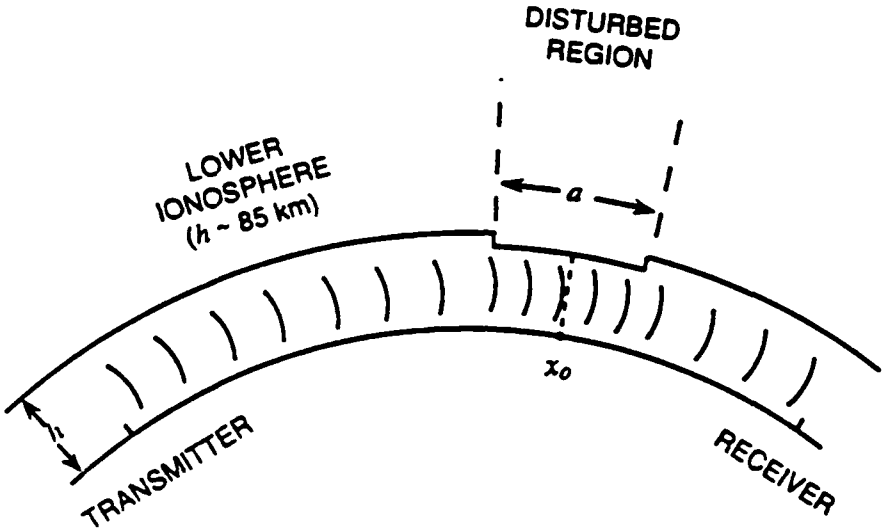

Figure 2-8: Sketch of the "pimple" on the bottom of the ionosphere [8].

transmitting the same series of three VLF signals [11]. Observations of signals used in the Omega radio navigation system have shown phase perturbations on the order of a microsecond. Assuming the signals propagate at approximately the speed of light in a vacuum (3×10^{10}cm/s) the resulting uncertainty in source-to-receiver distance would be ≈ 300 meters for a one microsecond phase difference. This amount does not significantly impact on the stated fix accuracy of the Omega system which is usually 1 to 4 km, but the amount of error introduced is important when using Differential Omega. Differential Omega increases the overall accuracy of a fix by assuming all signals received

have undergone the same amount of phase perturbation, an assumption not necessarily true because Trimpi effects are localized and can effect only one of the received signals. In addition, studies of Omega signals show that the amount of phase shift above 60° latitude is of the order of 10 microseconds. This translates into distance errors of 3000 meters which would double the uncertainty of the fix.[12]

There is great interest in learning more about how the reflective properties of the ionosphere can be changed. The precipitation of electrons as previously described is one method to change these properties of the ionosphere. Other methods include the direct heating of the ionosphere through the use of ground based high powered VLF transmitters and the introduction of chemicals to increase the ion concentration. One application of this work is development of an over-the- horizon radar which would use a patch of increased ionization in the atmosphere as a mirror [13]. Increased detection range and reduced chance of counter-detection are two features making such a system extremely desirable. A better understanding of the wave-particle interaction which results in electron precipitation is a step on the road to the development of this type of system.

III. THE ENVIRONMENT AND EQUATIONS OF MOTION

A. THE MAGNETOSPHERE

A good approximation for the earth's geomagnetic field is that of a dipole field located within the earth. The magnetopause is a boundary which separates the region where the earth's magnetic field dominates from the region where the action of the solar wind dominates. Within the magnetopause the dipole field approximation is valid. Outside the magnetosphere, the earth's field is distorted due to the solar wind. A bow shock forms on the side facing the sun as the solar wind causes the magnetosphere to be compressed. As the solar wind passes over and around the magnetosphere, a tail is created which has been observed to stretch out to $200R_e$, where R_e is the mean radius of the earth (6370 km). Figure 3-1 is a sketch of the magnetosphere and shows how the solar wind distorts the shape.[5]

This thesis will concentrate on the region inside the magnetosphere. This area includes the plasmasphere, made up of a "cold" background plasma and the "hot" plasma which makes up the earth's radiation belts. The background plasma is usually described as electrons and protons ranging in energy from .1 to 1 eV. They are in diffusive equilibrium and have densities from 10^4 particles/cm^3 at ionosphere heights (1000km) to 300-400 particles/cm^3 at the boundary of the plasmasphere. This boundary, called the plasmapause, was discovered through the study of naturally occurring whistlers and is characterized by a significant decrease in cold plasma density. The position of the plasmapause varies with solar activity: closer to the earth during magnetic

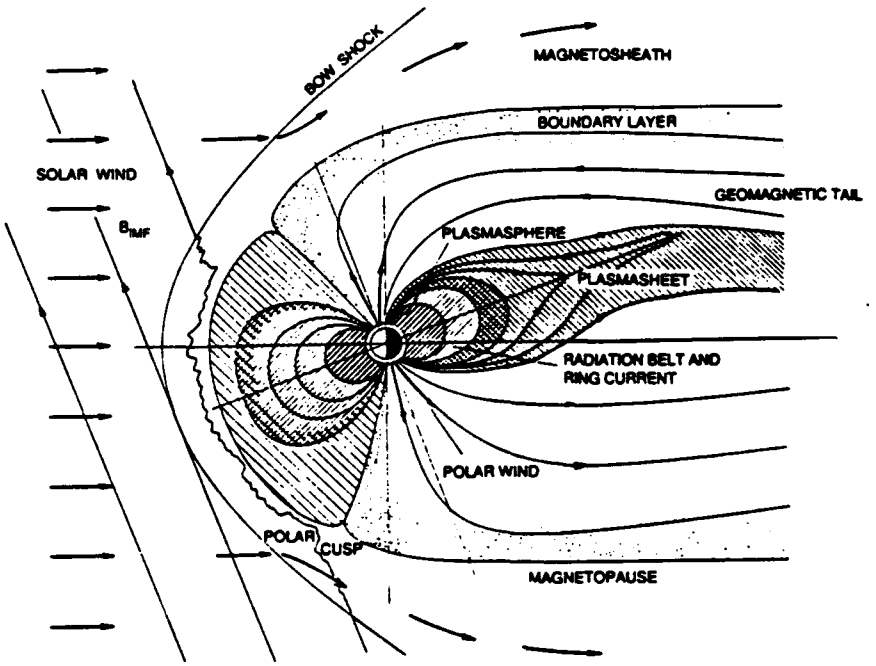

Figure 3-1: A schematic diagram of the Earth's magnetosphere in the noon-midnight plane [5].

storms ($2R_e$) and farther away ($7R_e$) after many days of little activity. The "hot" plasma includes electrons and protons having energies ranging from 10 kev to 100 Mev which are trapped by the geomagnetic field. They follow helical paths around field lines and bounce between magnetic conjugate points. Figure 3-2 is a sketch of the magnetosphere and includes examples of the helical paths these particles travel.[14]

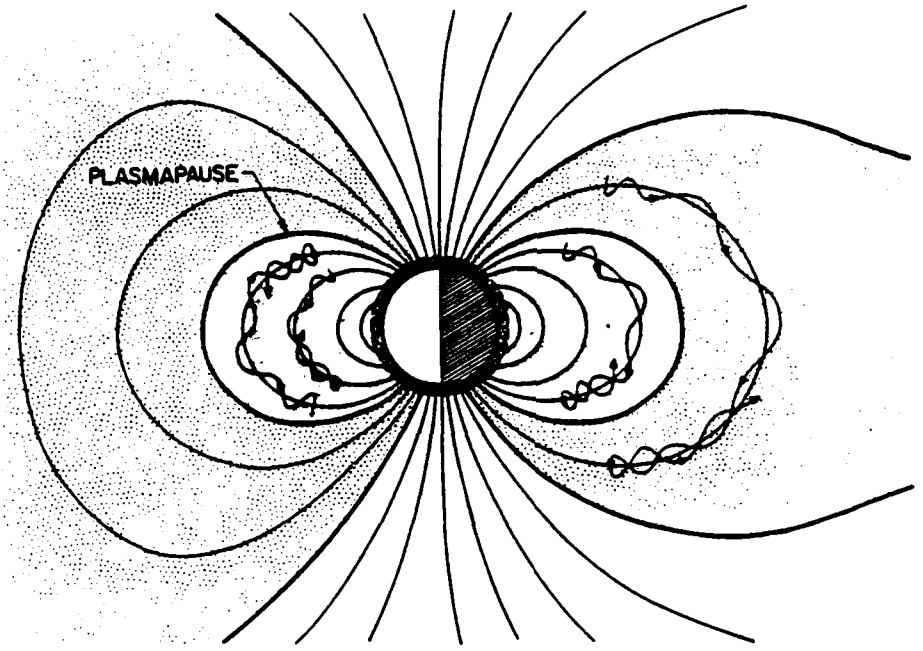

Figure 3-2: The magnetosphere including energetic particle trajectory [14].

B. THE MAGNETIC FIELD

The earth's magnetic dipole field is assumed to be embedded in the center of the earth with the axis tilted approximately 11° to the rotation axis. The field lines emerge from the south geographic pole and reenter the earth at the north geographic pole as shown in Figure 3-3. It is convenient to write the components of the geomagnetic field in terms of spherical coordinates, substituting geomagnetic latitude λ for the co-latitude θ. The field is symmetric in the ϕ direction. The equations describing the field components and the magnitude of the field are

$$B_r = -B_o\left[\frac{R_o}{r}\right]^3 2\sin\lambda \quad , \qquad 3\text{-}1$$

$$B_\lambda = B_o\left[\frac{R_o}{r}\right]^3 \cos\lambda \quad , \qquad 3\text{-}2$$

$$B = B_o\left[\frac{R_o}{r}\right]^3 \sqrt{1+3\sin^2\lambda} \quad . \qquad 3\text{-}3$$

where B_o is the magnitude of the field on the earth's surface at the geomagnetic equator (30,293nT) and R_o is the mean radius of the earth (6370 km). [14]

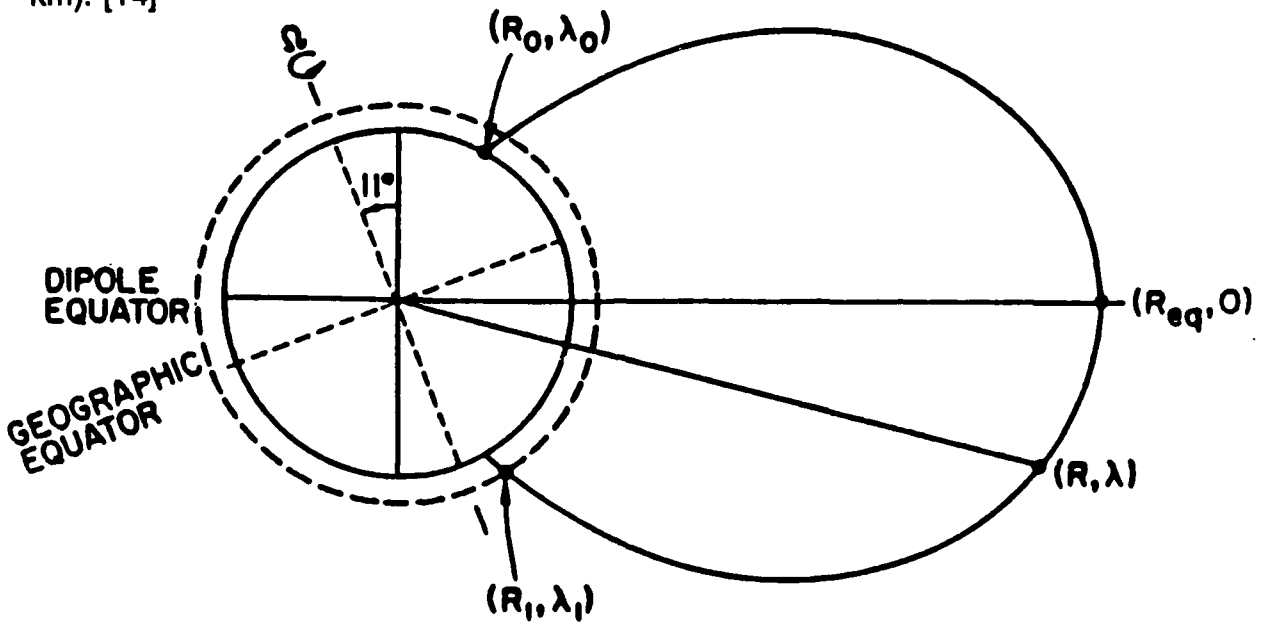

Figure 3-3: Dipole field used to represent Earth's magnetic field [14].

The equation for a dipole field line of force is $r = R_{eq}\cos^2\lambda$ in which R_{eq} is the radial distance to the field line when λ equals zero. The McIlwain L parameter is used to express a given field line in terms of the radial distance at which the field line crosses the geomagnetic equator,

$$L = \frac{R_{eq}}{R_o} \quad . \qquad 3\text{-}4$$

This parameter is a convenient way to label the field aligned ducts through which whistler-mode signals travel. [14]

C. ELECTRON MOTION IN THE MAGNETOSPHERE

The source of the high energy electrons in the radiation belts is not well known, although one theory is that they are deposited by the solar wind in the polar regions and then propagate down the magnetic field lines [9]. The motion of these electrons is governed by the Lorentz equation,

$$m\ddot{\vec{x}} = \vec{F} = -e(\vec{V} \times \vec{B}) \quad . \tag{3-5}$$

This force is always perpendicular to $\vec{V}$, the velocity vector of the electron and therefore the magnetic field $\vec{B}$ does no work on the electron. Only the component of the velocity which is perpendicular to $\vec{B}$ is affected by the force resulting in uniform circular motion around the magnetic field line. The radius of the cyclotron orbit is

$$r_c = \frac{mV_\perp}{eB} \tag{3-6}$$

where e is the charge of the electron, m is the mass of the electron, B is the magnitude of the magnetic field and $V_\perp$ is the component of the electron velocity perpendicular to $\vec{B}$. Assuming that $\vec{B}$ points into the paper, then the electron will rotate in a clockwise direction. When the $\vec{V}$ has a component parallel to $\vec{B}$, the electron follows a helical path around the field line. The angle that $\vec{V}$ makes with the magnetic field line is known as the pitch angle α

$$\alpha = \tan^{-1}\left[\frac{V_\perp}{V_\parallel}\right] \quad . \tag{3-7}$$

This angle will change as $V_\perp$ and $V_\parallel$ varies. When $V_\parallel$ equals zero, α is 90°. At this point the electron will stop its forward motion then travel in the opposite direction along the field line. It is as if the electron reflects off a mirror, while the direction of rotation remains the same.[5]

The magnitude of the earth's magnetic field, for a given field line, is at a minimum at the geomagnetic equator and increases as you move along the field line away from the equator. An electron moving up a field line from the equator will also see an increasing B field, but the electron executes many cyclotron gyrations in a distance where the amount of change in the field is small. This is known as an adiabatic change and it leads to the concept of the adiabatic invariant which states that the square of the transverse momentum of the electron divided by the magnitude of the field ($p_\perp^2/B$) is a constant. The field does not do work on the electron hence the speed of the electron must be constant and it can be written in terms of the velocity perpendicular and parallel to the geomagnetic field

$$V_o^2 = V_\perp^2 + V_\parallel^2 \quad , \qquad 3\text{-}8$$

where $V_o^2 = V_{\perp 0}^2 + V_{\parallel 0}^2$ is the speed of the electron at the geomagnetic equator. Assuming a coordinate system in which the z axis is aligned with the geomagnetic field, then the speed of the electron at z=0 is V_0 and the magnitude of the field is B_0. As a result of the adiabatic invariant,

$$\frac{V_\perp^2}{B(z)} = \frac{V_{\perp 0}^2}{B_0} \quad , \qquad 3\text{-}9$$

where B is a function of z. This relationship can then be used to find the parallel velocity of the electron,

$$V_\parallel^2 = V_0^2 - V_{\perp 0}^2 \frac{B(z)}{B_0} \quad . \qquad 3\text{-}10$$

As the field increases with increasing z eventually the right side of equation 3-10 will equal zero. At this point the electron reverses direction and heads back toward the equator while continuing to rotate around the field line in the same

direction. The equation of motion describing this deceleration can be expressed to first order in terms of the divergence of the field in the z direction [15]

$$\ddot{z} = \dot{V}_{\parallel} \approx -\frac{V_{\perp 0}^2}{2B_0}\frac{\partial B(z)}{\partial z} \quad . \qquad 3\text{-}11$$

When the electron reverses direction the pitch angle α equals 90^0. Using the adiabatic invariant leads to the definition of a mirror pitch angle α_m:

$$\sin^2\alpha_m = \frac{B_0}{B_m} \quad , \qquad 3\text{-}12$$

where B_m is the magnitude of the field when the electron mirrors [5]. Any electron with a pitch angle less than α_m as it crosses the geomagnetic equator will not mirror. The solid angle subtended by α_m defines a "loss cone". Electrons with pitch angles within the escape cone will mirror at a latitude where the field strength is greater than B_m. A higher magnitude means the mirror point is closer to the pole hence, these electrons will travel to a higher latitude before they reflect.

As the mirror latitude for an electron increases the altitude above the earth where reflection occurs decreases. As a result, electrons enter regions of the upper ionosphere of higher particle density and the possibility of energy loss through collision increases. If collisions do occur the electrons will precipitate out of their field aligned ducts. The wave-particle interaction which is thought to produce VLF emissions takes energy away from the electrons reducing their pitch angle. As a result, they precipitate out of the radiation belts in much high flux than is usually observed. This phenomenon is the Trimpi effect discussed in the last chapter. The derivation and simulations presented in the following

chapters will concentrate on the interaction which produces the increase in electron precipitation.

The equation of motion for electrons in a dipole field can be solved numerically using a desk top computer. Figure 3-4 shows the path of a trapped electron around the earth. In addition to the trapping of electrons, the inhomogeneity of the earth's magnetic field causes the electrons to drift in longitude as is clearly evident in the figure. The effect of this drift on the wave-particle interaction is not significant, and will not be considered in the simulations presented later.

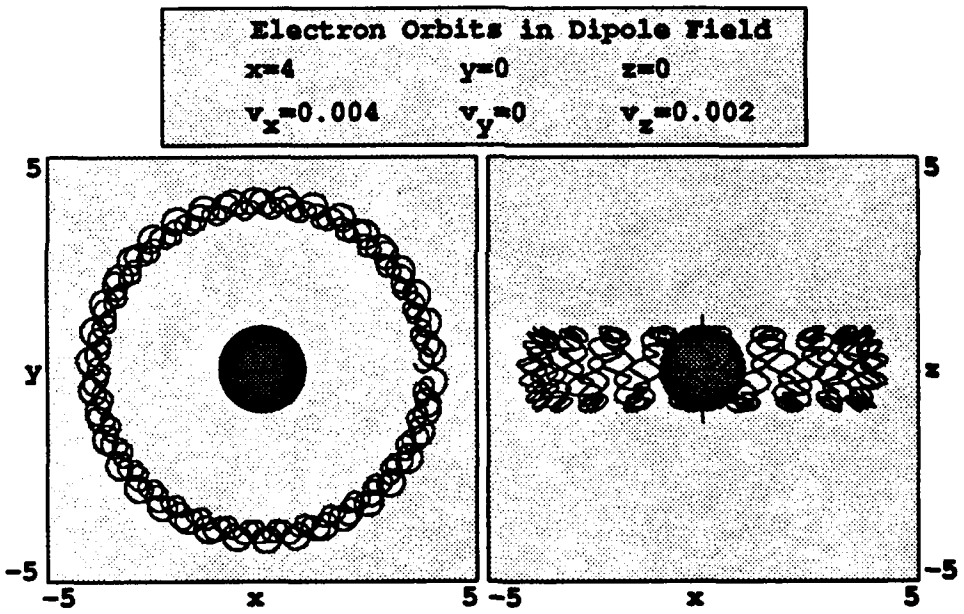

Figure 3-4: Plot of path taken by one electron in a dipole field. Bounce and drift motion are present.

D. ELECTRON EQUATIONS OF MOTION IN A MAGNETIC FIELD

The rest of this thesis will look at the wave particle interaction which amplify the incoming VLF wave and produce VLF emissions. In this model, the electrons which are executing cyclotron motion around the field lines gives up a small amount of energy to the propagating VLF wave [1]. When the Doppler-shifted wave frequency seen by the electrons equals the electron cyclotron frequency, the resonance condition can be expressed as

$$k\ V_{\parallel} = \omega - \Omega\,, \qquad 3\text{-}13$$

where k is the wave number of the VLF wave. For the case of waves propagating in the whistler mode, the electron cyclotron frequency, Ω, at the magnetic equator is much larger than the wave frequency, ω. As a result resonance only will occur when the electrons and the wave are traveling in opposite directions. Studies of many whistler spectrograms show a drop of greater than $10dB$ in wave intensity at a frequency approximately equal to one half the cyclotron frequency of the electrons at the magnetic equator [16]. VLF emissions are very narrow band indicating that the magnetic field the electrons travel through during resonance must be slowly varying over a long length. For these reasons, the interaction region is assumed to be the section of the field aligned duct that is near the magnetic equator as shown in Figure 3-5 [17].

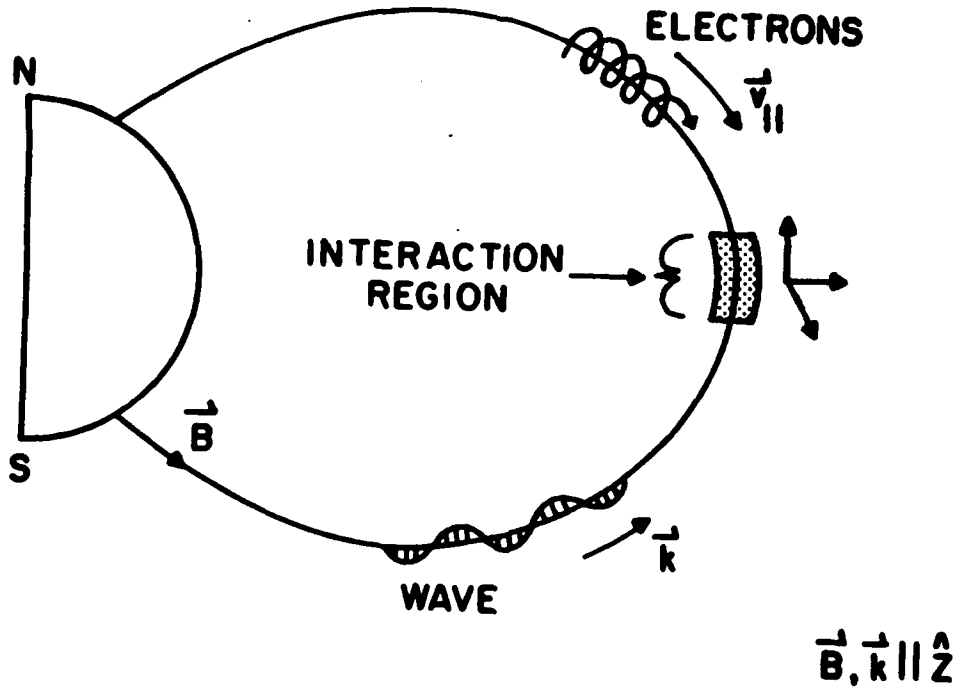

Figure 3-5: Sketch of the paths taken by the electrons and the wave including the interaction region (not to scale).

If the magnetic field is taken to be constant along the interaction region and $\vec{B}$ is parallel to the z axis, equation 3-5 can be written as

$$\dot{\vec{V}} = -\frac{e}{mc}(\vec{V} \times \vec{B}) \quad , \qquad 3\text{-}14$$

where $\dot{\vec{V}}$ is the electron acceleration expressed as the first derivative of velocity with respect to time. This vector equation can be written in component form resulting in three differential equations

$$\dot{V}_x = -\Omega V_y \quad , \quad \dot{V}_y = \Omega V_x \quad , \quad \dot{V}_z = 0 \quad . \qquad 3\text{-}15$$

The z component of velocity has no time-dependence, because the Lorentz force acts on that part of the electron velocity which is not parallel to the field.

A solution for these equations is

$$x = r_c\cos(\Omega t + \theta_0) \quad , \quad y = r_c\sin(\Omega t + \theta_0) \quad , \quad z = -v_z t \quad . \qquad 3\text{-}16$$

The term $r_c = V_\perp/\Omega$ and is the radius of the cyclotron orbit, $V_\perp$ is the transverse electron velocity, Ω is the cyclotron frequency, and θ_0 is the initial phase angle. Electrons with motion described by these equations will be referred to as the "hot" electrons. The resonance between these electrons and the counter propagating wave will be analyzed through the use of computer simulations.

IV. WAVE PARTICLE INTERACTION THEORY

A. THE BACKGROUND PLASMA

The propagation of the VLF wave through the interaction region is affected by the properties of the hot and cold plasma in the region. The "cold" background plasma is more dense ($\rho_c \approx 400/cm^3$) than the hot plasma described in the previous chapter. The cold background plasma contains non-resonance electrons that affect the wave dispersion relation while hot electrons amplify the wave. Without considering the effect of the VLF wave, the cold plasma executes cyclotron motion around the magnetic field lines. This motion is described by the Lorentz force equation and $\vec{r}$ is given by

$$\vec{r} = \frac{V_{c\perp}}{\Omega}[-\cos(\Omega t), \sin(\Omega t), 0] \quad , \qquad 4\text{-}1$$

where $r = V_{c\perp}/\Omega$ is the radius of gyration, and the initial phase angle is taken to be zero. Since the cold electrons are non-resonant, the small z velocity component can be ignored. The cold electrons rotate in a clockwise direction when looking along the magnetic field line with a velocity equal to,

$$\vec{V}_c = V_{c\perp}[\sin(\Omega t), \cos(\Omega t), 0] \quad . \qquad 4\text{-}2$$

When the VLF wave is included, the Lorentz force equation is written as

$$\dot{\vec{V}}_c = -\frac{e}{m}\left[\vec{E}_w + \frac{\vec{V}_c}{c} \times (\vec{B}_w + \vec{B})\right] \quad , \qquad 4\text{-}3$$

where $\vec{E}_w$ and $\vec{B}_w$ are the electric and magnetic field vectors of the propagating VLF wave. The magnitude of B_w is much less than the geomagnetic field in the

interaction region and can therefore be neglected here. In component form, equation 4-3 is

$$\dot{V}_{cx} + \Omega V_{cy} = -\frac{e}{m} E_{wx} \quad , \qquad 4\text{-}4$$

$$\dot{V}_{cy} - \Omega V_{cx} = -\frac{e}{m} E_{wy} \quad . \qquad 4\text{-}5$$

Assuming that the incoming VLF wave is right-hand circularly polarized, the fields are;

$$\vec{E}_w = E_w[\cos(\psi), -\sin(\psi), 0] \; , \quad \vec{B}_w = B_w[\sin(\psi), \cos(\psi), 0] \quad . \qquad 4\text{-}6$$

where the phase of the propagating wave is $\psi = kz - \omega t + \phi_0$. The wave travels from the south pole to the north pole as previously shown in Figure 3-5. The wave propagation vector is taken to be parallel to the geomagnetic field and the wave acts as driving force for the cold electrons. As a result, their steady-state motion must have the same space and time dependence as the driving wave. If the form for the cold electron velocity is taken to be

$$\vec{V}_c = V_{c\perp}[\sin(\psi), \cos(\psi), 0] \quad , \qquad 4\text{-}7$$

and this form is then used in equations 4-4 and 4-5, two equations which include $V_{c\perp}$ result:

$$V_{c\perp}\omega \cos(\psi) - \Omega V_{c\perp} \cos(\psi) = \frac{e}{m} E_w \cos(\psi) \quad , \qquad 4\text{-}8$$

$$V_{c\perp}\omega \sin(\psi) - \Omega V_{c\perp} \sin(\psi) = \frac{e}{m} E_w \sin(\psi) \quad . \qquad 4\text{-}9$$

Both equations can be solved simultaneously resulting in an expression for $V_{c\perp}$,

$$V_{c\perp} = -\frac{eE_w}{m(\Omega - \omega)} \quad . \qquad 4\text{-}10$$

The current generated by the motion of these cold electrons can now be written as

$$\vec{J}_c = \frac{e^2 \rho_c E}{m(\Omega-\omega)}[\sin\psi, \cos\psi, 0] \quad , \tag{4-11}$$

where ρ_c is the density of the cold electrons.

This current density, along with the expressions for E_w and B_w, can then be inserted into Ampere's Law and Faraday's Law

$$\vec{\nabla}\times\vec{B}_w = \frac{4\pi}{c}\vec{J}_c + \frac{1}{c}\frac{\partial \vec{E}_w}{\partial t} \quad , \tag{4-12}$$

$$\vec{\nabla}\times\vec{E}_w = -\frac{1}{c}\frac{\partial \vec{B}_w}{\partial t} \quad . \tag{4-13}$$

Assuming that the VLF field envelope, E_w, B_w and ϕ, are constant in time and space, these Maxwell equations can be simplified to

$$B_w ck = E_w \omega + \frac{4\pi e^2 \rho_c E_w}{m(\Omega-\omega)} \quad , \tag{4-14}$$

$$E_w ck = B_w \omega \quad . \tag{4-15}$$

The index of refraction of the interaction region is defined as $n = ck/\omega$. As a result, equation 4-15 shows that $B_w = nE_w$. Using this relationship and substituting into equation 4-14 results in an expression for n^2,

$$n^2 = \frac{c^2k^2}{\omega^2} = 1 + \frac{\omega_c^2}{\omega(\Omega-\omega)} \quad , \tag{4-16}$$

where the plasma frequency for the cold electrons, $\omega_c = 4\pi e^2 \rho_c / m$. The expression for the index of refraction given in Chapter II (equation 2-3) follows directly from 4-16 because $\omega_c \gg \omega$ and $\omega_c \gg \Omega$. Equation 4-16 is the exact dispersion relation for the VLF wave in a cold, magnetized plasma [14].

B. THE WAVE EQUATION

The next step is to develop a wave equation that describes the evolution of the VLF wave envelope. It would include the factors that contribute to the growth of the wave envelope as it passes through the interaction region. Referring back to the two Maxwell equations used in the last section, the current density must now include the hot electrons

$$\vec{J} = \vec{J}_c + \vec{J}_h \ , \qquad 4\text{-}17$$

where $\vec{J}_h = -eV_{h\perp}[-\sin(\theta)\ ,\ \cos(\theta)\ ,\ 0]$ is the current for a single hot electron, $V_{h\perp}$ is the transverse velocity of a hot electron and $\theta = \Omega t + \theta_0$ is the phase of the electron cyclotron motion. The variation of the wave envelope in space and time is assumed to be small over one wavelength [13],

$$\dot{E}_w \ll \omega E_w \ , \ \dot{\phi} \ll \omega\phi \ , \ E'_w \ll kE_w \ , \ \phi' \ll k\phi \ .$$

This slowly-varying amplitude and phase approximation is appropriate when the VLF envelope describes a narrow-band whistler mode.

Returning to Ampere's Law, equation 4-12, and using equation 4-6 to represent the VLF wave results in the following vector equation:

$$\partial_z B_w[-\cos(\psi),\sin(\psi),0]+B_w(k+\partial_z\phi)[\sin(\psi),\cos(\psi),0] - \qquad 4\text{-}18$$

$$\frac{1}{c}\partial_t E_w[\cos(\psi),\sin(\psi),0]+\frac{E_w}{c}(-\omega+\partial_t\phi)[\sin(\psi),\cos(\psi),0] = \frac{4\pi}{c}\vec{J} \ ,$$

where $\partial_z(..) = \partial(..)/\partial z$ and $\partial_t(..) = \partial(..)/\partial t$. Defining two unit vectors,

$$\hat{\varepsilon}_1 = [\sin\psi\ ,\cos\psi\ ,0] \ \ , \ \ \hat{\varepsilon}_2 = [\cos\psi\ ,-\sin\psi\ ,0] \ \ , \qquad 4\text{-}19$$

and projecting Ampere's Law onto these orthogonal unit vectors results in two scalar first-order differentia' equations,

$$ckB_w - \omega E_w + cB_w\partial_z\phi + E_w\partial_t\phi = \frac{\omega_c^2 E_w}{\Omega-\omega} - 4\pi e V_{h\perp}\cos(\psi+\theta) \quad , \qquad 4\text{-}20$$

$$c\partial_z B_w + \partial_t E_w = -4\pi e V_{h\perp}\sin(\psi+\theta) \quad . \qquad 4\text{-}21$$

Using $nE_w = B_w$ and the dispersion relation, 4-16, further simplifies these equations to obtain,

$$ncB_w\partial_z\phi + B_w\partial_t\phi = -4\pi e n V_{h\perp}\cos(\psi+\theta) \quad , \qquad 4\text{-}22$$

$$nc\partial_z B_w + \partial_t B_w = -4\pi e n \sin(\psi+\theta) \quad . \qquad 4\text{-}23$$

At this point it is convenient to define the quantity b:

$$b = \frac{eB_w}{mc}\exp(i\phi) \quad . \qquad 4\text{-}24$$

The complex field b has units of inverse seconds (s^{-1}), and is $\approx 1/s$, when the VLF wave amplitude is at a maximum (10pT). It is anticipated that the VLF fields will not be bigger than this value. Taking the partial derivative of b with respect to z and t in accordance with the chain rule results in

$$\partial_z b = \frac{e}{mc}\exp(i\phi)[\partial_z B_w + iB_w\partial_z\phi] \quad , \qquad 4\text{-}25$$

$$\partial_t b = \frac{e}{mc}\exp(i\phi)[\partial_t B_w + iB_w\partial_z\phi] \quad . \qquad 4\text{-}26$$

These expressions can then be used to organize 4-22 and 4-23 into a complex equation,

$$(nc\partial_z + \partial_t)b = -\frac{i4\pi e^2}{m} V\exp[-i(\zeta+\theta)] \, , \qquad 4\text{-}27$$

where $\zeta = kz - \omega t + \Omega t$ is the longitudinal electron phase and $V=nV_{h\perp}/c$ is the dimensionless transverse electron velocity.

The current in Ampere's Law is for a single hot electron in the presence of the incoming VLF wave. The current for a beam of hot electrons is obtained by averaging over the transverse velocity V, the transverse phase θ, and the longitudinal phase ζ. The average is symbolized by <...>, and must be weighted by the hot electron beam density ρ_h. The wave equation 4-27 for a beam of hot electrons is then as

$$(nc\partial_z + \partial_t)b = -i\omega^2{}_h\langle V\exp[-i(\zeta+\theta)]\rangle \,, \qquad 4\text{-}28$$

where $\omega^2{}_h = 4\pi e^2\rho_h/m$ is the hot electron plasma frequency. When the VLF wave envelope is spatially flat over many wavelengths, $\partial_z b$ is zero and the wave equation can be written as

$$\dot{b} = -i\omega^2{}_h\langle V\exp[-i(\zeta+\theta)]\rangle \,. \qquad 4\text{-}29$$

As the incoming VLF wave enters the interaction region it encounters a random distribution of hot electrons whose z motion is described by $z_h = z_{h0} - V_{hz}t$. The current contains the factor <exp[-i(kz_0)]> where z_0 is the initial random position of a hot electron. The number of hot electrons in the average <...> describing one wavelength of the incoming wave is $\approx 10^{13}$ so that the current will average to a value very close to zero. The right side of equation 4-29 is small regardless of the value of ω_h and therefore, the VLF wave is not amplified. What is needed is a description of how the positions of the hot electrons evolve as the wave passes. The dynamical equations for the hot electrons in the presence of the VLF wave are derived next.

C. DEVELOPMENT OF ELECTRON EQUATIONS OF MOTION

The motion of the hot electrons in the presence of the incoming field, like the motion of the cold electrons, is governed by the Lorentz force equation

$$\dot{\vec{V}}_h = -\frac{e}{m}\left[\vec{E}_w + \vec{V}_h \times (\vec{B}_w + \vec{B})\right] \quad , \qquad 4\text{-}30$$

but unlike the analysis used for the cold electrons, the magnetic field of the incoming wave B_w is not dropped. The geomagnetic field is assumed to be of the form $\vec{B} = [0,0,B]$, and E_w and B_w are taken from equation 4-6, so that equation 4-30 becomes

$$\dot{V}_{hx} = -\frac{e}{m}\left[E_w\left[\frac{n}{c}V_{hz}\right]\cos\psi + \frac{B}{c}V_{hy}\right] \quad , \qquad 4\text{-}31$$

$$\dot{V}_{hy} = -\frac{e}{m}\left[-E_w\left[\frac{n}{c}V_{hz}\right]\sin\psi - \frac{B}{c}V_{hx}\right] \quad , \qquad 4\text{-}32$$

$$\dot{V}_{hz} = -\frac{e}{m}\left[E_w\frac{n}{c}(V_{hx}\cos\psi - V_{hy}\sin\psi)\right] \quad , \qquad 4\text{-}33$$

where $\psi = kz - \omega t + \phi$. The hot electron velocity in the x-y plane can be expressed in polar coordinates in terms of $V_{h\perp}$ and $\theta_\perp$,

$$V_{hx} = -V_{h\perp}\sin(\theta_\perp) \quad , \quad V_{hy} = V_{h\perp}\cos(\theta_\perp) \quad . \qquad 4\text{-}34$$

Expressions for $\dot{V}_{hx}$ and $\dot{V}_{hy}$ can be obtained from equation 4-34 through the use of the chain rule. After making the appropriate substitutions into equations 4-31 and 4-32 the following expressions result:

$$\dot{V}_{hz} = \frac{eE_w}{mc}nV_{h\perp}\sin(\theta_\perp + \psi) \quad , \qquad 4\text{-}35$$

$$\dot{V}_{h\perp} = \frac{eE_w}{mc}(c - V_{hz}n)\sin(\theta_\perp + \psi) \quad , \qquad 4\text{-}36$$

$$\dot{\theta}_\perp = \Omega + \frac{eE_w}{mc} V_{h\perp}^{-1} (c - V_{hz} n)\cos(\theta_\perp + \psi) \quad . \tag{4-37}$$

Making the definition $\theta_\perp = \Omega t + \theta$ the argument of the sin and cos functions in equations 4-35, 4-36 and 4-37 becomes

$$\theta_\perp + \psi = kz_h - \omega t + \Omega t + \theta + \phi \quad . \tag{4-38}$$

The electron phase is $\zeta = kz_h - \omega t + \Omega t$. Using $\dot{\theta}_\perp = \Omega + \dot{\theta}$, the hot electron equations of motion take the following form;

$$\ddot{z}_h = \frac{eB_w}{mc} V_{h\perp} \sin(\zeta + \theta + \phi) \quad , \tag{4-39}$$

$$\dot{V}_{h\perp} = \frac{eB_w}{nm}\left[1 - \frac{nV_{hz}}{c}\right]\sin(\zeta + \theta + \phi) \quad , \tag{4-40}$$

$$\dot{\theta} = \frac{eB_w}{nmV_{h\perp}}\left[1 - \frac{nV_{hz}}{c}\right]\cos(\zeta + \theta + \phi) \quad , \tag{4-41}$$

where $B_w = nE_w$ and $\ddot{z}_h = \dot{V}_{hz}$.

Looking at the definition for ζ, it is clear that $\ddot{\zeta} = k\ddot{z}$. Making this substitution into equation 4-39 results in

$$\ddot{\zeta} = \frac{eB_w}{mc} \omega \frac{nV_{h\perp}}{c} \sin(\zeta + \theta + \phi) \quad . \tag{4-42}$$

Equation 4-42 can be further simplified using the definitions for a complex field $b = |b|e^{i\phi}$ where $|b| = eB_w/mc$ and where $V = nV_{h\perp}/c$. The expression for the electron phase is now

$$\ddot{\zeta} = V\omega|b|\sin(\zeta + \theta + \phi) \quad . \tag{4-43}$$

Equation 4-43 will be referred to as the pendulum equation for the electrons.

Equations 4-40 and 4-41 can also be simplified through the use of the phase and group velocity of the VLF wave

$$V_p = \frac{c}{n} = \frac{\omega}{k}, \quad V_g = \frac{d\omega}{dk} \quad , \qquad 4\text{-}44$$

where $ck = n\omega$ and n is the index of refraction in the interaction region. Using the index for the case of $\omega_c \gg \omega, \Omega$,

$$n \approx \frac{\omega\omega_c}{\sqrt{\omega(\Omega-\omega)}} \quad , \qquad 4\text{-}45$$

the group velocity can be evaluated in terms of n as

$$V_g \approx 2\frac{c}{n}\left[1-\frac{\omega}{\Omega}\right] \quad . \qquad 4\text{-}46$$

The phenomenon of a "cutoff" frequency was described in Chapter III, and is defined as one half the electron cyclotron frequency, $\Omega/2$, at the magnetic equator. The simulations presented in the next chapter will assume that the frequency of the incoming VLF wave is $\omega = \Omega/2$. When this is substituted into equation 4-46, it is found that $V_g \approx V_p$. At resonance and at cutoff, $V_{hz} = -V_p$ so that the electrons and the wave travel at equal speeds in opposite directions. Using $-c/n$ for V_{hz} in equations 4-40 and 4-41 as well as the definitions for the magnitude of $|b|$ and V results in

$$\dot{V} = 2|b|\sin(\zeta + \theta + \phi) \quad , \qquad 4\text{-}47$$

$$\dot{\theta} = \frac{2|b|}{V}\cos(\zeta + \theta + \phi) \quad . \qquad 4\text{-}48$$

The equations of motion for the electron in the presence of the VLF wave equations, 4-43, 4-47, 4-48, along with the wave equation, 4-29, are now in a convenient form to integrate numerically and understand further.

A final modification to the equation for $\ddot{\zeta}$ comes when the electron phase velocity is defined as $v = \dot{\zeta}$. This allows all the important equations describing

the hot electrons and the VLF field to be in the form of first-order differential equations. The collected set of equations are

$$\dot{v} = V\omega|b|\sin(\zeta + \theta + \phi) \quad , \tag{4-49}$$

$$\dot{\zeta} = v \quad , \tag{4-50}$$

$$\dot{V} = 2|b|\sin(\zeta + \theta + \phi) \quad , \tag{4-51}$$

$$\dot{\theta} = \frac{2|b|}{V}\cos(\zeta + \theta + \phi) \quad , \tag{4-52}$$

$$\dot{b} = -i\omega_h{}^2 \langle V e^{-i(\zeta + \theta)} \rangle \quad . \tag{4-53}$$

V. SIMULATIONS AND DISCUSSION

A. EXPLANATION OF NUMERICAL INTEGRATION METHODS

The equations presented at the end of Chapter IV are non-linear, so that the only method of solution is through the use of numerical techniques. This process can be carried out on a desk- top computer. Assuming a small finite time-step, Δt, the electron equations can be written as

$$\Delta v = V\omega|b|\sin(\zeta + \theta + \phi)\Delta t \quad , \tag{5-1}$$

$$\Delta\zeta = v\Delta t \quad , \tag{5-2}$$

$$\Delta V = 2|b|\sin(\zeta + \theta + \phi)\Delta t \quad , \tag{5-3}$$

$$\Delta\theta = \frac{2|b|}{V}\cos(\zeta + \theta + \phi)\Delta t \quad , \tag{5-4}$$

The equations for Δv and $\Delta\zeta$ each have a factor of ω which is not present in the equations for ΔV or $\Delta\theta$. The value of ω is $\approx 10^4/s$, and it is therefore anticipated that the equation for v will evolve much faster than the last two equations. As a result, the first two equations will be numerically integrated using the fourth-order Runge-Kutta method [18] while the simpler, more efficient Euler-Cromer method [18] will be used to integrate the last two equations. Each equation describes how the values for each variable change over the short time interval Δt. The simulation will use this process to keep track of and plot how the electrons evolve over time.

The wave equation is also a first-order differential equation in time, but V, ζ and θ on the right-hand side of 4-53 must be averaged over all the sampled hot electrons. In the simulation, the values for v, ζ, V and θ will be found first for

each of the hot electrons. The average values for V, ζ and θ will then be determined, and used in finding a new value for b. For a small finite time-step Δt, the wave equation can be written in complex form as

$$\Delta b = -i\omega_h{}^2 \langle V e^{-i(\zeta + \theta)} \rangle \Delta t \quad . \tag{5-5}$$

The computer actually evaluates this equation as written in real and imaginary components. The actual equations used by the computer are

$$\Delta b_r = -\omega_h{}^2 \langle V \sin(\zeta + \theta + \phi) \rangle \Delta t \quad , \tag{5-6}$$

$$\Delta b_i = -\omega_h{}^2 \langle V \cos(\zeta + \theta + \phi) \rangle \Delta t \quad . \tag{5-7}$$

where $b = b_r + ib_i$. Using these real and imaginary components in the equations for the electron motion results in

$$\Delta v = V\omega[b_r \sin(\zeta + \theta) + b_i \cos(\zeta + \theta)]\Delta t \quad , \tag{5-8}$$

$$\Delta \zeta = v \Delta t \quad , \tag{5-9}$$

$$\Delta V = 2[b_r \sin(\zeta + \theta) + b_i \cos(\zeta + \theta)]\Delta t \quad , \tag{5-10}$$

$$\Delta \theta = \frac{2}{V}[b_r \cos(\zeta + \theta) - b_i \sin(\zeta + \theta)]\Delta t \quad . \tag{5-11}$$

These are the equations which will be integrated by the computer using the methods mentioned above.

B. INITIAL CONDITIONS

The position of each electron and the amplitude and phase of the VLF wave can now be determined, but the initial values for each of the variables is required for integration. As stated in Chapter IV, there are many electrons ($\approx 10^{13}$) in a volume of the interaction region one wave length long. It is not possible to integrate this many electrons so that a smaller sampling will be

used. These electrons are assumed to be in a beam with a uniform distribution in initial ζ and initial θ ranging between $-\pi$ to π. The initial values for v will be determined by the distribution functions $f(v)$, where σ_v characterizes the spread in $f(v)$, while v_0 characterizes the function $f(v)$. The distribution function $g(V)$ provides the initial distribution in the dimensionless transverse velocity V with σ_V characterizing the spread in $g(V)$, and V_0 characterizes the position of $g(V)$. Since the equation of motion for $\dot{\theta}$ involves V^{-1}, it is important that $g(V)$ approach zero for small V. The loss cone for mirroring electrons in the ionosphere assures this property.

The initial VLF field is $b_r = b_o$ and $b_i = 0$ so that the initial phase angle is $\phi(0) = 0$. The plasma frequency, ω_h, depends on the density of hot electrons at the time of the VLF interaction in the Earth's ionosphere and can vary significantly with the level of magnetic activity. When $\rho_h = 1/m^3$, $\omega_h = 50/s$ [19] provides a typical value for the ionosphere, but other values will be examined in the simulations. The length of time, T, over which the interaction takes place is typically a fraction of a second, based on the observation that whistler traces are approximately one second long. The interaction occurs in a relatively small portion of the total length of a field aligned duct, therefore the run time for a simulation should be a fraction of that total time.

C. INTERACTIONS FOR MONO-ENERGETIC BEAM

The first set of simulations are for the case were $f(v)$ and $g(V)$ are delta-functions, and all the electrons start with the same initial value for $v_0 = 0$ and $V_0 = 1$ corresponding to a pitch angle of $\pi/4$. Figure 5-1 shows the results of this simulation for a VLF wave with a frequency $\omega = 10^4/s$. The plot on the left shows the electron phase velocity, v, versus the electron phase, ζ. In the

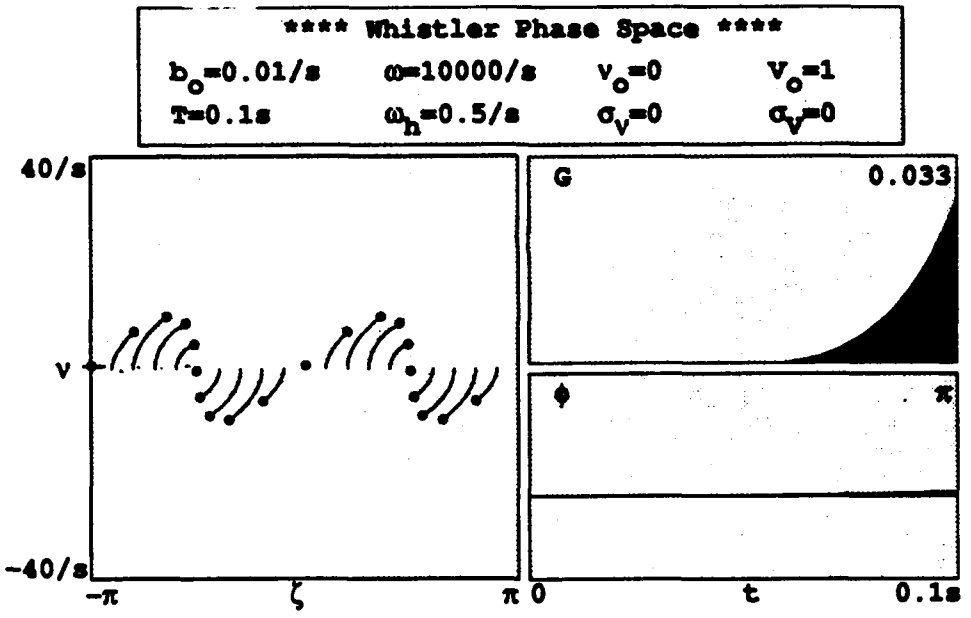

Figure 5-1: Electron phase-space, gain and phase for weak fields and low gain.

phase-space plot, the path and final positions for each of the electrons are plotted. Those paths which move down in v indicate that these electrons are giving up energy to the wave, while those moving up in v are increasing in energy, removing it from the wave. In this case, almost as many electrons go up in energy as go down. The electrons clearly bunch around two values of ζ in one wavelenght of the VLF wave. The right-hand plots show how the gain, *G*, and phase of the VLF wave , ϕ, develop over the course of the interaction. The gain is a measure of how the wave amplitude changes over time and is defined as

$$G = \frac{|b(t)|^2}{|b(0)|^2} - 1 \quad . \qquad 5\text{-}12$$

The average on the right side of the wave equation, 4-53, provides the driving

current for the VLF wave. When there is bunching the average is close to zero, and the wave does not grow significantly. When bunching finally occurs near the end of the undulator, the gain increases to a final value of $G = 3\%$. The size of $|b|$ is small and does not increase significantly because ω_h is small. The phase of the VLF wave, ϕ, does not change significantly during the interaction.

In Figure 5-2, the same initial conditions are used but the plots of G and ϕ are replaced by a plot showing the evolution of V and θ on the right. Throughout the integration, these variables remain very close to their initial values.

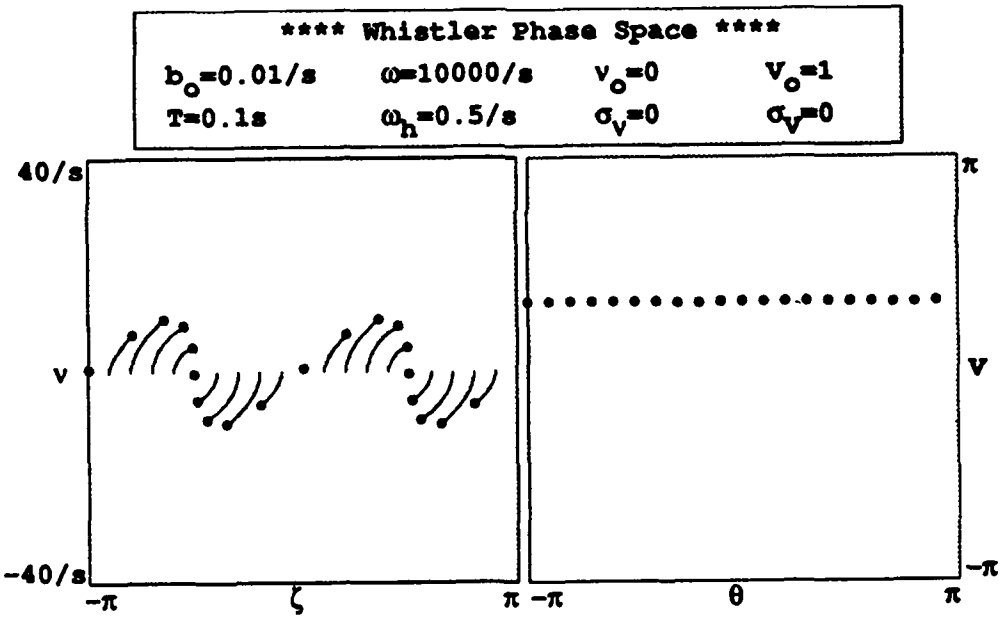

Figure 5-2: Electron phase-spaces (ζ,v) and (θ,V) for weak fields and low gain.

In Figure 5-3 the hot plasma frequency is increased to $\omega_h = 5/s$ resulting in an increase in gain for this interaction. At the start of the interaction the electrons begin to bunch as in the previous cases. This causes ϕ to increase

so that the point around which the electrons bunch advances a little along ζ. The larger driving current increases the amplitude of the VLF wave and the

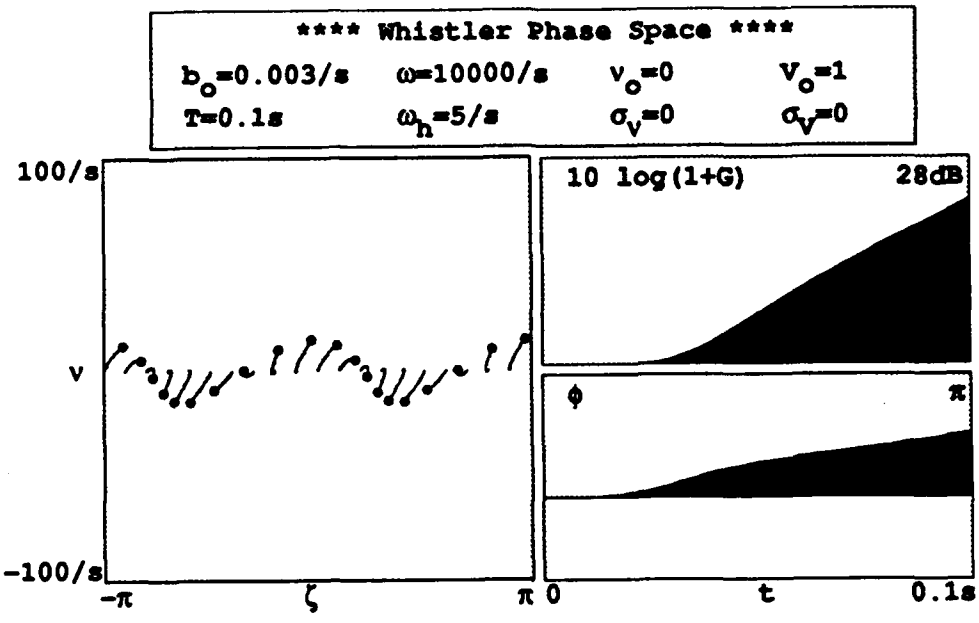

Figure 5-3: Electron phase-space, gain and phase for weak fields and high gain.

gain. The gain increases exponentially in time and reaches a final value of *28dB*. The phase increases significantly to nearly π at the end of the interaction. The final size of $|b|$ is still small but it is much greater than the initial value due to high gain. This set of conditions produced high gain in relatively weak fields.

Figure 5-4 shows that again the variables V and θ did not evolve significantly.

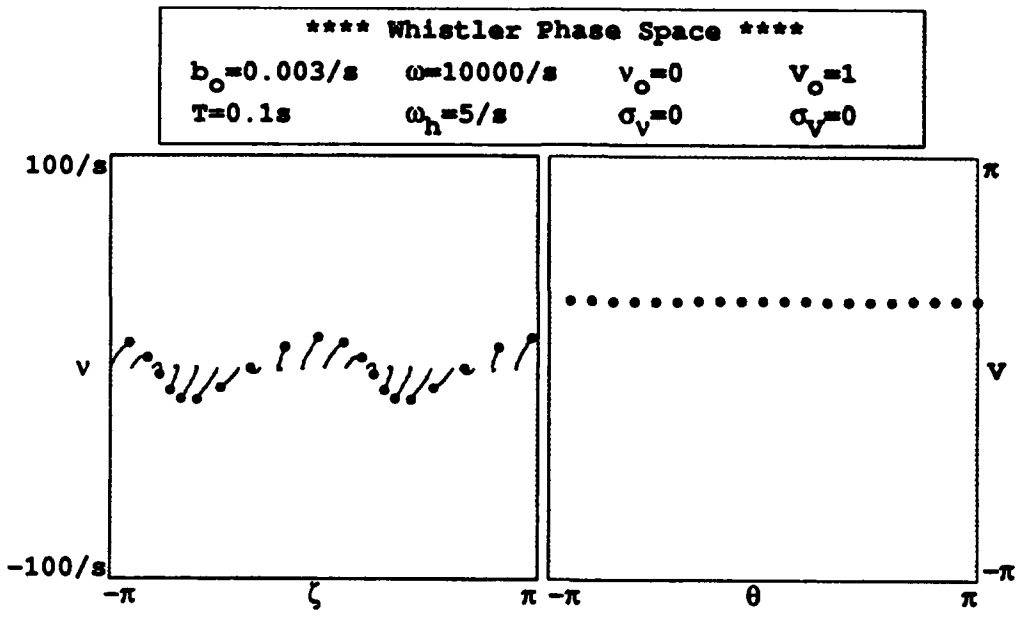

Figure 5-4: Electron phase-spaces (ζ,v) and (θ,V) for weak fields and high gain.

The next set of simulations study the effect of large VLF field strengths. In Figure 5-5, the value of $b_0 = 0.1/s$ is increased by a factor of ten over the value in Figure 5-1 while $\omega_h = 0.5/s$ stays the same. This larger initial field causes the electrons to over-bunch as shown in the electron phase-space plot on the left. As the bunching starts, the gain increases, but as the over-bunching continues the rate of increase in the gain slows and finally levels off at the end of the simulation. As the electrons move past their bunched positions, they take energy away from the VLF wave reducing the amplitude. The final gain is only $G = 0.4\%$ for the same value of ω_h as in Figure 5-1, but it has decreased because of large $|b|$. This also leads to almost no change in ϕ.

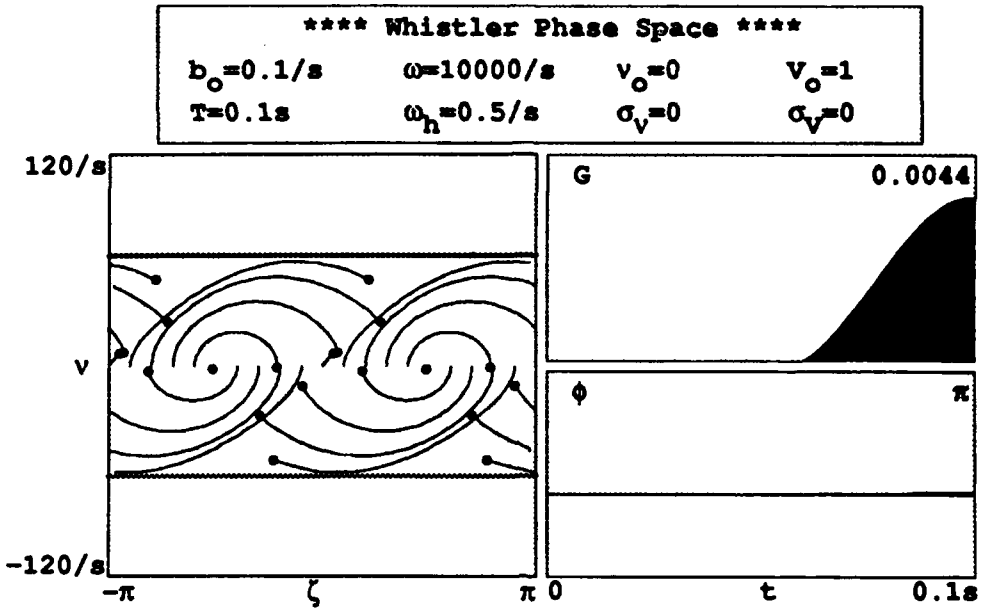

Figure 5-5: Electron phase-space, gain and phase for strong fields and low gain.

In the phase-space plot of Figure 5-5, the boundary lines define the maximum radius within the closed orbit region. The boundary lines are located at $\Delta v = \pm 2\sqrt{|b|\omega V}$ above and below resonance. The frequency at which the electrons orbit about fixed points within the closed orbit region is known as the "synchrotron frequency", $v_S = \sqrt{|b|\omega V}$. It is possible that the gain can also oscillate at this synchrotron frequency.

In Figure 5-6 the plot of electron velocity versus θ does not evolve during the interaction.

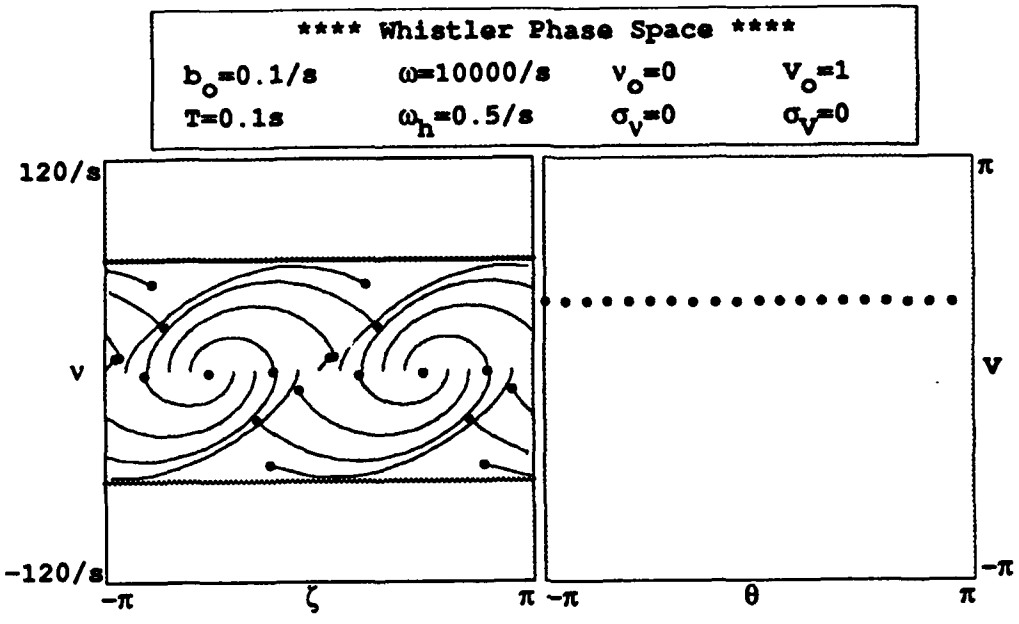

Figure 5-6: Electron phase-spaces (ζ,v) and (θ,V) for strong fields and low gain.

Figure 5-7 shows the results of high gain with $\omega wubh = 5/s$ and a strong field $b_0 = 0.3/s$. The electrons over-bunch again, but the gain is much higher because ω_h is bigger. The over-bunching limits the gain to $G = 5.9dB$ compared to $G = 29dB$ in Figures 5-3 and 5-4. Some of the electrons crossed the lower boundary of the closed-orbit region because the value of $|b|$ is larger at $t \approx 0.06s$ than the final value used to draw the boundary lines at $\pm 2\sqrt{|b|\omega V}$. The gain plot shows a tendency for the gain to oscillate at the synchrotron frequency. The phase change, ϕ, is large as expected with a large value of ω_h. The data collected on VLF waves in the magnetosphere indicates the interaction involves strong fields with high-gain. In Figure 5-8, the plot of electron transverse velocity V versus θ still does not evolve during the interaction.

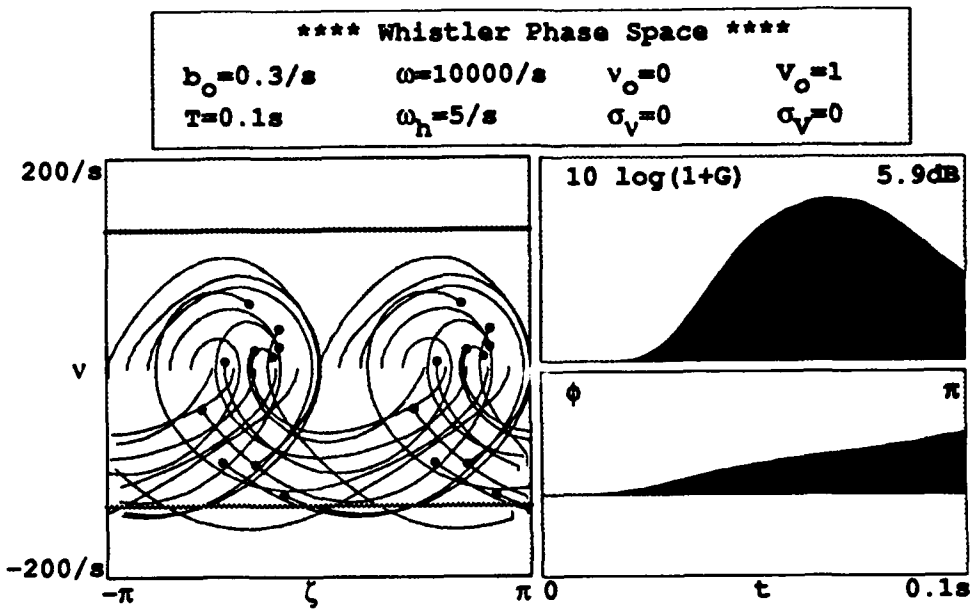

Figure 5-7: Electron phase-space, gain and phase for strong fields and high gain.

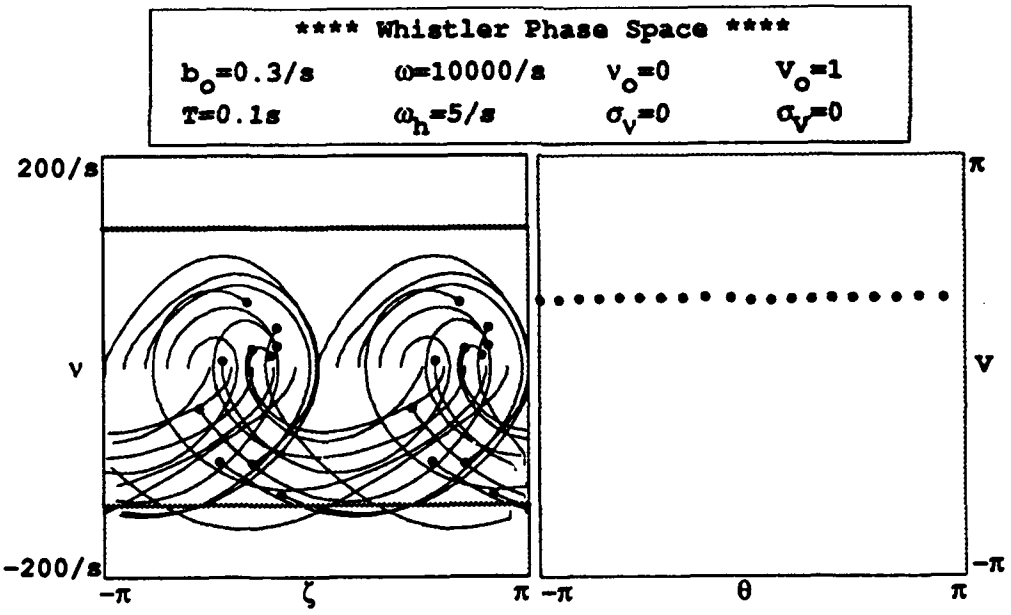

Figure 5-8: Electron phase-spaces (ζ,v) and (θ,*V*) for strong fields and high gain.

Figure 5-9 shows the same strong-field, high-gain simulation as in Figure 5-7, but the electrons are moved off-resonance to $v_0 = 130/s$. The electrons follow open orbit paths which are outside the closed orbits region. The large

initial value for v_0 results in a large initial ζ where $\zeta = \zeta_0 + v_{0t}$. This large ζ oscillates so quickly that the average of $\dot{\zeta}$ is zero over one phase ϕ. This results in weak coupling to the VLF field and therefore the gain in this case is smaller, $G = 3.8dB$, than in Figure 5-7 where $G = 5.9dB$. The plot of V versus θ in Figure 5-10 does not evolve during the interaction.

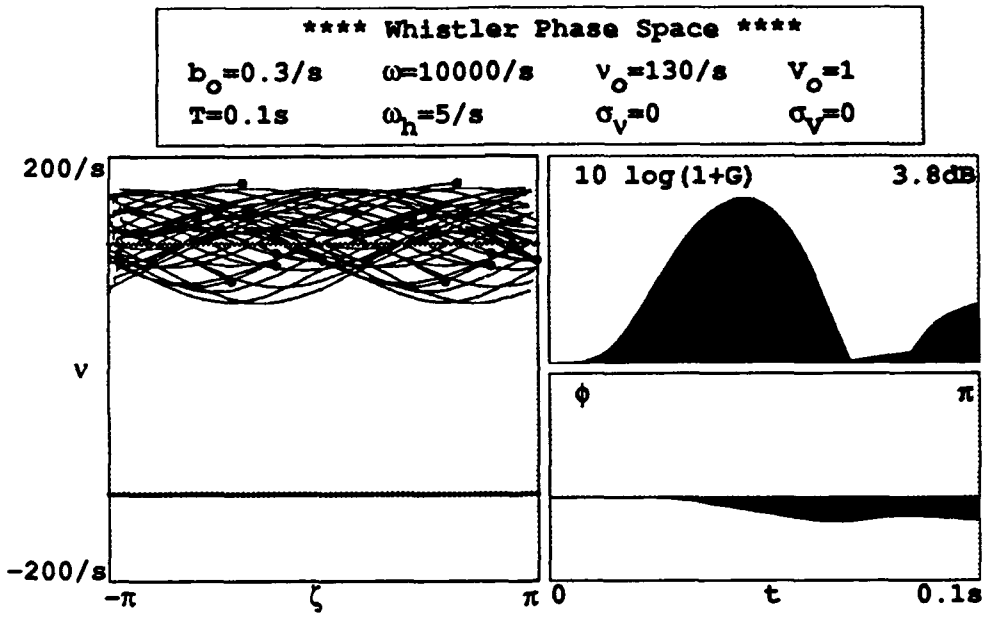

Figure 5-9: Electron phase-space, gain and phase for strong fields and high gain starting off-resonance.

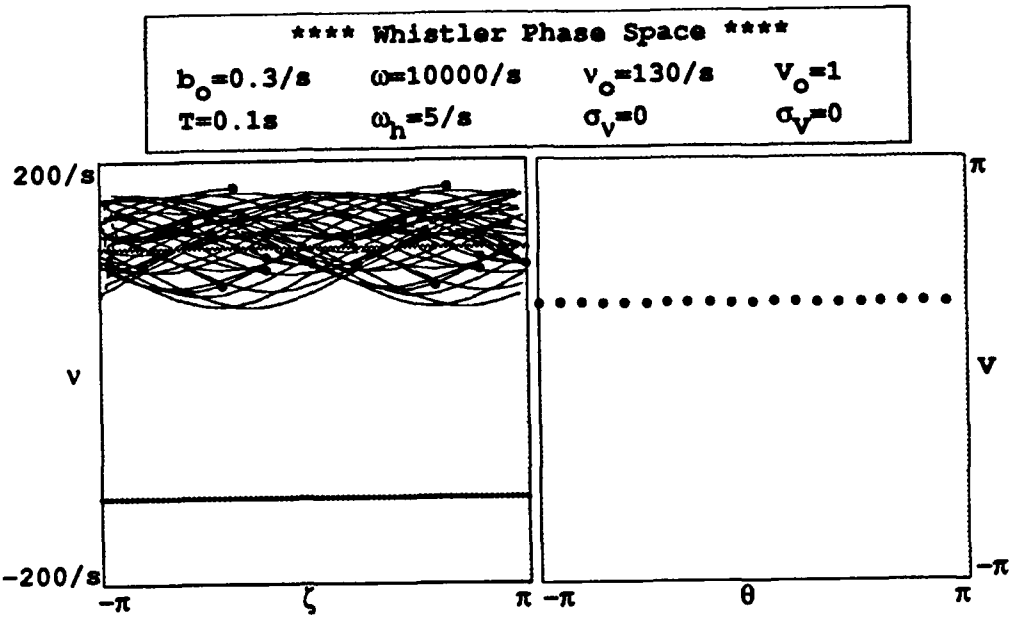

Figure 5-10: Electron phase-spaces (ζ,v) and (θ,V) for strong fields and high gain starting off-resonance.

D. SIMULATIONS USING DISTRIBUTIONS

The electrons in the magnetosphere are not monoenergetic. Studies of data obtained from spacecraft flying through the magnetosphere indicate that the density of electrons between E_h = 750eV and E_h = 50keV varies as E_h^{-n} where n can have values from 1.5 to 3.5 [20]. There are many more electrons with low energies than there are at higher energies for this type of distribution function. Using the relationship between energy and velocity means the number density of electrons in terms of velocity is V_h^{-2n}. This function can also represent the distribution of hot electrons in terms of V_{hz} and $V_{h\perp}$ because these quantities are directly related to the electron velocity. The initial phase velocity of the electrons, v_0, is directly related to the initial velocity in the z direction, V_{hz}. When the electrons have a value of v_0 which is significantly away from resonance, there is poor coupling to the VLF field, and the gain is small as

shown in Figure 5-9. As a result only those electrons with v_0 in a narrow band around resonance need be considered. The size of this narrow band around v_0 is related to the spread in V_{hz} through the relationship,

$$\frac{\Delta v_0}{\omega} = \frac{\Delta V_{hz}}{c/n} \quad , \qquad 5\text{-}16$$

where c/n is the velocity of resonant electrons. When $\Delta v = 500/s$ and $\omega = 15000/s$ the spread around the resonant velocity is only ±3%. This is such a small portion of the overall distribution, E_h^{-n}, that the initial electron phase velocity distribution, $f(v_0)$, can be represented by a linear function with a negative slope. Smaller values of v_0 will have a higher probability, because lower velocities are more likely than higher velocities for this type of distribution function. The actual $f(v_0)$ used is triangular in shape with a full-width-at half-maximum, σ_v, wider than the window of v_0 values used. The result is a sloped distribution in $f(v_0)$ used to start the *simulation electrons*.

The distribution function $g(V)$ used to select the initial values for V must reflect the properties of the velocity distribution discussed above as well as the distribution in pitch angles α because $V = nV_{h\perp}/c$. The lower boundary for $g(V)$ is defined by the loss cone, α_m. Electrons with pitch angles less than α_m precipitate out of the field aligned ducts and are not present to contribute to wave growth. Because this angle is so small, $V_{h\perp} \approx V_h$ and $V_{hz} \approx V_h$. The resonant velocity is defined as c/n, therefore, at α_m

$$V = \frac{V_{h\perp}}{c/n} \approx \alpha_m \quad . \qquad 5\text{-}17$$

An exponential distribution will be used for $g(V)$ with the peak at V_0 which

corresponds to $\alpha = \alpha_m$. The full width at half maximum, $\sigma_V = 1$, corresponds to a pitch angle $\alpha = 45^0$, where $V_{h\perp} = V_{hz}$.

In Figure 5-11, the simulation is run for initial parameters which are intended to represent the environment in the interaction region. The initial values for v and V for each electron is determined using $f(v)$ and $g(V)$. The value the hot electron plasma frequency is taken to be $\omega_h = 25/s$ corresponding to a density of hot electrons, $\rho_h = .18/m^3$ in the magnetosphere. The initial VLF field is $b_0 = .01/s$ which is lower than the strong field cases previously presented in Figures 5-7 through 5-10. The spread in V_z is found using 5-16 and is equal to ±3% of the resonant velocity. A large number of particles (8000) are used in the simulations, therefore only the final positions are plotted in phase-space.

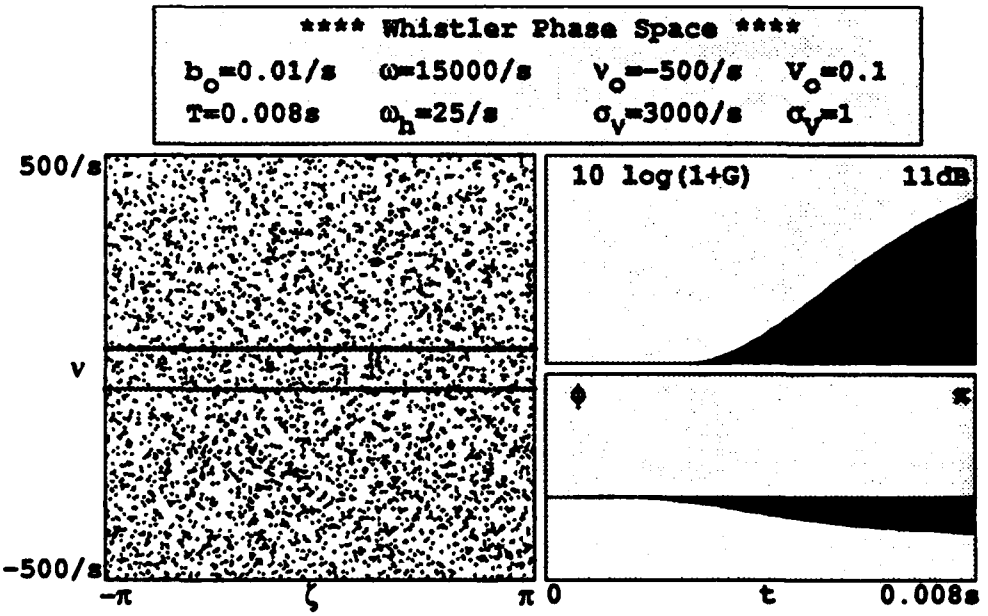

Figure 5-11: Electron phase-space gain and phase for magnetospheric initial conditions, short interaction time.

In phase-space, particles with lower energy are at the bottom. In accordance with the description of $f(v)$ and $g(V)$, there are more electrons in the lower half or the phase-space plot than in the upper half. Although this may be difficult to perceive from just looking at the plot, the simulation checks for this by counting the number of electrons in a small strip at the top and bottom of phase-space and taking the ratio of these numbers. In Figure 5-11, the gain grows exponentially and the phase does not change significantly.

When the simulation runs for a longer integration time, T, as in Figure 5-12, the gain saturates then begins to oscillate. This shows the saturation of the VLF wave in strong VLF fields.

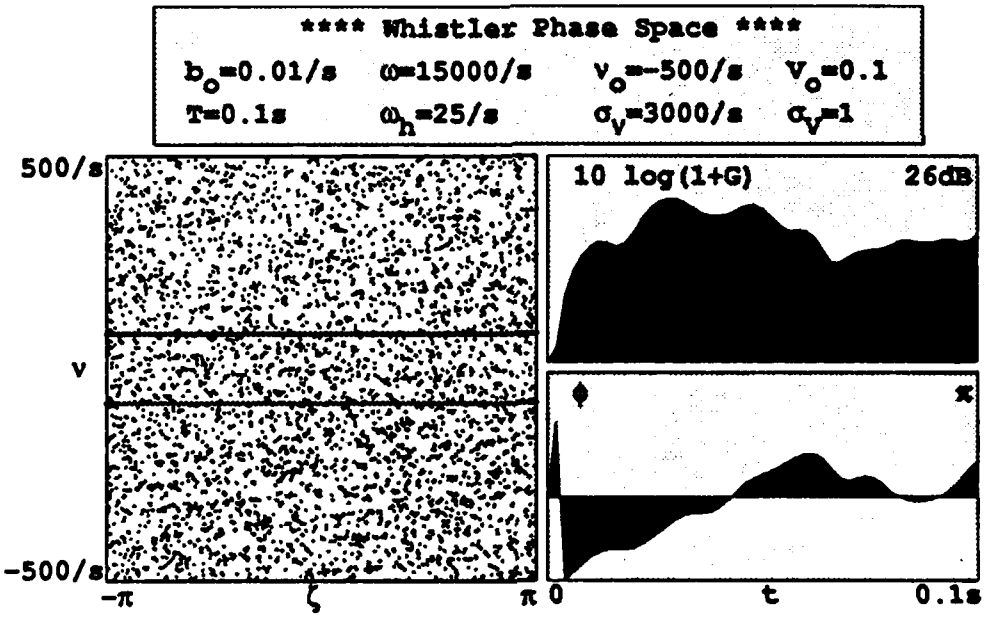

Figure 5-12: Electron phase-space gain and phase for magnetospheric initial conditions, long interaction time.

VI. SUGGESTIONS FOR FUTURE WORK

A. IMPROVEMENTS TO THE SIMULATION

The simulation at this point in development assumes the geomagnetic field is homogeneous throughout the interaction region. A better approximation would include a factor in the electron equations of motion which accounts for the increasing field seen by the electrons as they move to higher latitudes. This increase in the field decelerates the electrons in the z direction and changes the VLF resonance condition. The expression for this deceleration was presented in Chapter III,

$$\ddot{z} = -\frac{V_{h\perp}^2}{2B}\frac{\partial B(z)}{\partial z} \quad , \tag{6-1}$$

where $B(z)$ is the geomagnetic field as a function of position z [15]. In the absence of the VLF interaction, the velocity of the hot electrons at the magnetic equator is constant in time, and can be expressed in component form as

$$V_{h0}^2 = V_{hz}^2 + V_{h\perp}^2 \tag{6-2}$$

Taking the time derivative of both sides in 6-2, and using the expression for $\ddot{z} = \dot{V}_{hz}$ results in an expression for the transverse components

$$\dot{V}_{h\perp} = \frac{V_{hz} V_{h\perp}}{2B}\frac{\partial B(z)}{\partial z} \quad . \tag{6-3}$$

These factors can now be added to the expressions found previously for $\ddot{z}_h$ and $\dot{V}_{h\perp}$ giving,

$$\ddot{z}_h = \frac{eB_w}{mc} V_{h\perp} \sin(\zeta + \theta + \phi) - \frac{V_{h\perp}^2}{2B} \frac{\partial B(z)}{\partial z} \quad , \qquad 6\text{-}4$$

$$\dot{V}_{h\perp} = \frac{eB_w}{nm} \left[1 - \frac{nV_{hz}}{c} \right] \sin(\zeta + \theta + \phi) + \frac{V_{hz} V_{h\perp}}{2B} \frac{\partial B(z)}{\partial z} \quad . \qquad 6\text{-}5$$

The field around the equator as a function of z is

$$B(z) = B_0 \left[1 + \frac{9z^2}{12R_e^2} \right] \quad , \qquad 6\text{-}6$$

where R_e is the radius of the earth [21]. The development from here on is the same as previously presented in Chapter IV.

This addition will cause the cyclotron frequency of the hot electrons to change as the electrons travel along their helical paths. As a result, the electrons move in and out of resonance with the wave. When the field is assumed to be homogeneous the interaction turns on and off abruptly. By including the effect of the changing field the interaction turns on and off gradually in a similar way to that in the magnetosphere.

The distribution functions $f(v)$ and $g(V)$ present another area which needs further investigation. An accurate description of the initial energies of the resonant electrons will improve the output of the simulation. This problem is complicated because these functions vary significantly with magnetic activity. If all other initial conditions were accurately known, various types of distribution functions could be studied and then compared to experimental data in hopes of predicting the electron density.

In all the cases examined in Chapter V, the equations for $\dot{V}$ and $\dot{\theta}$ did not evolve. Future simulations may not need to integrate these equations and still produce meaningful results. In that case, this type of simulation would closely

resemble those used in the study of Free Electron Lasers (FEL). Each would integrate a pendulum equation, following the development of the electron phase velocity and the coupling to the field. Even if the simulation integrates the single equation, the distribution function $g(V)$ must still be included. In the FEL, all electrons have the same $V_\perp$ which is directly related to V, but that is not the case in the case of VLF interactions in the magnetosphere.

B. COMPARISON TO FREE ELECTRON LASERS

The theory and simulations presented up to this point are all in an attempt to describe what is a naturally occurring effect. The process used to amplify light in the Free Electron Laser (FEL) is very similar to the amplifying process described for VLF waves in the magnetosphere. Any parallels in theory are beneficial because an FEL is a laboratory device making it much easier to study topics of mutual interest. The areas common to both subjects include:

1. The FEL amplifier couples the radiation coming from electrons accelerated in helical orbits to a transverse laser light field. The electrons are accelerated as a result of a transverse magnetic field, but the kind of paths they follow is the same as for electrons in the magnetosphere.
2. The radiation produced by the FEL is very narrow band and can result in a gain of several thousand.
3. The evolution of the electron phase-space can be described using the pendulum equation: $\dot{v} = |a|\cos(\zeta + \phi)$, where $\ddot{\zeta} = \dot{v}$. Simulations used to investigate aspects of FEL theory output the same type of displays as used in Chapter V.

4. An FEL operating in the microwave region makes use of a waveguide resulting in a dispersion relation, $n\omega = kc$.[22]
5. The electron distribution function is important to FEL and the VLF interaction.
6. When the transverse field in the FEL is tapered at the ends of the interaction length, the effect is similar to that when the magnetic field varies in the magnetosphere.
7. Advanced effects such as saturation, particle trapping and non-linear dynamics are all common to both systems.

VII. CONCLUSIONS

An overall description of whistler waves and the related topic of VLF emissions is presented in Chapter II along with a discussion of how these phenomena can change the properties of the ionosphere and thereby degrade the performance of communication and navigation systems used by the U. S. Navy. A method using whistlers to remotely determine the electron density in the plasmasphere is also presented here. The theory of wave-particle interaction is presented to explain how the waves are amplified. The propagation properties of the magnetosphere are presented resulting in a dispersion relation for waves traveling through a cold, magnetized background plasma. The equations of motion for electrons making helical paths around magnetic field lines are presented at the end of Chapter III.

A self-consistent wave equation for VLF signals passing through a cold, magnetized plasma is developed in Chapter IV. A new set of equations for the resonant electrons in the presence of the VLF field is also presented at the end of the chapter. This set of nonlinear differential equations are solved using numerical integration carried out on a desk top computer. The first set of simulations are for a monoenergetic beam of resonant electrons. Weak and strong initial field amplitudes are examined for both high and low gain cases. The outputs show the electron phase-space paths as well as plot of gain and the phase of the field as a function of time. For weak fields, the electrons bunch around two points in one wave length of the VLF signal. The amount of gain is governed by the density of the hot electrons. In strong fields, the electrons over-bunch, taking energy away from the VLF field. The gain

saturates, then oscillates at the synchrotron frequency. Distribution functions to represent the density of the hot electrons in the magnetosphere are used to provide a more realistic set of simulations. A large number of electrons are needed so only the final positions are plotted in phase-space. The gain grows exponentially, reaches saturation and then begins to oscillate.

A number of suggestions are presented in Chapter VI to make the simulation more realistic. Many aspects of Free Electron Laser theory are very similar to that presented for wave-particle interactions in the magnetosphere. These similarities are listed at the end of Chapter VI.

LIST OF REFERENCES

[1] R. A. Helliwell, *Whistlers and Related Phenomena*, Stanford University Press, 1965.

[2] L. O. R. Story, "Whistlers", *Scientific American*, v. 194, 1, January 1956.

[3] D. L. Carpenter and R. L. Smith, "Whistler Measurements of Electron Density in the Magnetosphere," *Reviews of Geophysics*, v. 2, 3, August 1964.

[4] R. N. Sudan and J. Denavit, "VLF Emissions from the Magnetosphere," *Physics Today*, v. 26, 12, December 1973.

[5] G. K. Parks, *Physics of Space Plasmas, An Introduction*, Addison-Wesley Publishing Company, 1991.

[6] D. L. Carpenter, "Whistler Studies of the Plasmapause in the Magnetosphere," *Journal of Geophysical Research*, v. 71, 693, February 1966.

[7] K. Molvig and others, "Self-Consistent Theory of Triggered Whistler Emissions," *Journal of Geophysical Research*, v. 93, A6, June 1988.

[8] W. L. Poulsen, "Modeling of Very Low Frequency Wave Propagation and Scattering within the Earth-Ionosphere Waveguide in the Presence of Lower Ionospheric Disturbances," Ph.D. Dissertation, Stanford University, November 1991.

[9] M. J. Rycroft, "Cause and Effects of Interaction between Energetic Electrons and Whistler-Mode Waves in the Coupled Magnetosphere-Ionosphere-Atmosphere System," paper presented at Electromagnetic Wave Propagation Symposium, Bergen, Norway, 28-31 May 1990.

[10] R. A. Helliwell, J. P. Katsufrakis and M. L. Trimpi, "Whistler-Induced Amplitude Perturbations in VLF Propagation," *Journal of Geophysical Research*, v. 78, 22, August 1973.

[11] *American Practical Navigator*, Volume I, Defense Mapping Agency Hydrographic/Topographic Center, 1984.

[12] U. S. Inan and others, "Subionospheric VLF/LF Phase Perturbations Produced by Lightning-Whistler Induced Particle Precipitations," *Journal of Geophysical Research*, v. 90, A8, August 1985.

[13] P. A. Kossey and others, "Artificial Ionospheric Mirrors (AIM)," paper presented at Electromagnetic Wave Propagation Symposium, Bergen, Norway, 28-31 May 1990.

[14] U. S. Inan, "Non-Linear Gyroresonant Interactions of Energetic Particles and Coherent VLF Waves in the Magnetosphere," Ph.D. Dissertation, Stanford University, August 1977

[15] J. D. Jackson, *Classical Electrodynamics*, 2nd edition, John Wiley and Sons, 1975.

[16] D. L. Carpenter, "Ducted Whistler-Mode Propagation in the Magnetosphere; A Half-Gyrofrequency Upper Intensity Cutoff and Some Associated Wave Growth Phenomena," *Journal of Geophysical Research*, v. 73, 9, May 1968.

[17] R. A. Helliwell, "Theory of Discrete VLF Emissions from the Magnetosphere," *Journal of Geophysical Research*, v. 72, 19, October 1967.

[18] H. Gould and J. Tobochnik, *An Introduction to Computer Simulation Methods, Part 1*, Addison-Wesley Publishing Company, 1988.

[19] R. A. Helliwell and T. L. Crystal, "A Feedback Model of Cyclotron Interaction between Whistler-Mode Waves and Energetic Electrons in the Magnetosphere,"

Journal of Geophysical Research, v. 78, 31 November 1973.

[20] M. A. Schield and L. A. Frank, "Electron Observations Between the Inner Edge of the Plasma Sheet and the Plasmasphere," *Journal of Geophysical Research*, v. 75, 28, October 1970.

[21] U. S. Inan and R. A. Helliwell, "Terrestial Versus Jovian VLF Chorus; A Comparative Study," *Journal of Geophysical Research*, v. 88, A8, August 1983.

[22] W.B. Colson, "Classical Free Electron Laser Theory", Chapter 5 in *Free Electron Laser Handbook*, W.B. Colson, C. Pellegrini and A. Renieri (eds.), North-Holland Physics, Elsevier Science Publishing Co. Inc., The Netherlands 1990.

INITIAL DISTRIBUTION LIST

1.	Defense Technical Information Center Cameron Station Alexandria, Virginia 22304-6145	2
2.	Library, Code 52 Naval Postgraduate School Monterey, California 93943-5002	2
3.	Professor William B. Colson, Code PH/Cw Department of Physics Naval Postgraduate School Monterey, California 93943-5000	9
4.	Professor S. Gnanalingam, Code PH/Gn Department of Physics Naval Postgraduate School Monterey, California 93943-5000	1
5.	Professor K. E. Woehler Code PH/Wh Chairman, Department of Physics Naval Postgraduate School Monterey, California 93943-5000	1